NASA CONTRACTOR REPORT

NASA CR-1788

GEOMETRIC, AERODYNAMIC, AND KINEMATIC CHARACTERISTICS OF TWO TWIN KEEL PARAWINGS DURING DEPLOYMENT

by Paul M. Kenner, Frederic T. Churchill, and Ralph B. Holt

Prepared by
VOUGHT MISSILES AND SPACE DIVISION
LTV AEROSPACE CORPORATION
Dallas, Texas 75222
for Langley Research Center

NATIONAL AERONAUTICS AND SPACE ADMINISTRATION • WASHINGTON, D. C. • AUGUST 1971

1. Report No.	2. Government Accession No.	3. Recipient's Catalog No.
NASA CR-1788		

4. Title and Subtitle	5. Report Date
GEOMETRIC, AERODYNAMIC, AND KINEMATIC CHARACTERISTICS OF TWO TWIN KEEL PARAWINGS DURING DEPLOYMENT	August 1971
	6. Performing Organization Code

7. Author(s)	8. Performing Organization Report No.
PAUL M. KENNER, FREDERIC T. CHURCHILL AND RALPH B. HOLT	
	10. Work Unit No.

9. Performing Organization Name and Address	11. Contract or Grant No.
VOUGHT MISSILES AND SPACE DIVISION LTV AEROSPACE CORPORATION DALLAS, TEXAS 75222	NAS1-6957
	13. Type of Report and Period Covered
12. Sponsoring Agency Name and Address	Contractor Report
NATIONAL AERONAUTICS AND SPACE ADMINISTRATION WASHINGTON, D. C. 20546	14. Sponsoring Agency Code

15. Supplementary Notes

16. Abstract

The paper presents the results of an analysis of flight test data on two intermediate size (5000 lb payload) twin keel parawings. Kinematic data on various points on each canopy were determined along with establishing forces for two stages of inflation. Transient aerodynamics produced pressure differentials as high as five times the dynamic pressure of the free stream. Local structural failures are attributed to impulsive arresting of spanwise expansion and abrupt reversals in curvature during chordwise expansion.

17. Key Words (Suggested by Author(s))	18. Distribution Statement
Parawing deployment dynamics, kinematic and aerodynamic data, flight tests and data reduction, twin keel, 5000 lb. payload	Unclassified - Unlimited

19. Security Classif. (of this report)	20. Security Classif. (of this page)	21. No. of Pages	22. Price*
Unclassified	Unclassified	68	$3.00

*For sale by the National Technical Information Service, Springfield, Virginia 22151

FOREWORD

This report was prepared by members of the Structures and Materials Section, Vought Missiles and Space Division, LTV Aerospace Corporation, under NASA Contract NAS1-6957, DSI No. 10, Parawing Structural and Data Analysis, Phase I, and is based upon work performed between March 1969 and September 1969. The work was sponsored by the NASA Langley Research Center under the management of Mr. D. L. Clemmons, Jr., Manager, Parawing Project Office. Technical direction was provided by Mr. V. L. Alley, Jr., of the Engineering Analysis Branch of the Systems Engineering Division. Mr. W. E. Craig, Jr., was technical representative to the contracting officer.

GEOMETRIC, AERODYNAMIC, AND KINEMATIC CHARACTERISTICS OF TWO TWIN KEEL PARAWINGS DURING DEPLOYMENT

By Paul M. Kenner, Frederic T. Churchill
and Ralph B. Holt

Vought Missiles and Space Division

SUMMARY

This study seeks to determine the geometric, aerodynamic and kinematic characteristics of the deployment phase of two intermediate size (5000 lb payload), twin keel, parawings by analysis of flight test data. The flight tests were conducted at the D.O.D. Joint Parachute Test Facility, El Centro, California in October 1968. Both tests employed a parawing deployment sequence consisting of five stages of inflation.

The motion of various points on each canopy was determined during the critical events from first stage disreef through fourth stage inflation. These data are presented in curves showing displacement, velocity, and acceleration of a point as functions of time. The displacement data were taken directly from ground camera records. The velocity and acceleration were calculated by differentiation.

Canopy geometry and aerodynamic pressure distributions were determined for each flight at the critical times of first and second stage inflation. The critical times were determined by analysis of data from the test vehicle accelerometers, suspension line load cells, and photographic recordings. The aerodynamic pressure distributions were determined from the measured shapes and velocities by conventional approximation techniques combining closed form solutions, empirical results, and test data for similar conditions. The results are presented as pressure distribution curves on various cross sections and as spanwise and chordwise load distributions and their integrals. The time histories of the projected drag areas were determined from payload photographic records throughout all phases of deployment.

INTRODUCTION

The development of technology for flexible recovery devices having a capability for gliding flight has been pursued by the parawing research program at the NASA Langley Research Center for over a decade (reference 1). From the standpoint of maneuver capability and descent rate, parawings are clearly superior to parachutes of equal canopy area. However, the realization of the apparent potential of parawings depends upon their ability to meet competitive weight and packing volume requirements while maintaining an adequate margin against tearing.

Packing volume can be minimized by employing an all-flexible parawing, that is, a configuration with no rigid supporting structure. Consequently, a considerable volume of research has been devoted to the determination of the performance and deployment characteristics of various all-flexible designs. The status of the research in this area through September 1968 is summarized in reference 2. In particular, the objectives and scope of the contract work being done by Northrup Ventura for Langley Research Center is presented. In the performance of their contractual obligations, Northrup Ventura encountered some difficulties with the deployment of the intermediate size (5000 lb payload) twin keel parawing. Repeated instances of canopy damage were experienced at intermediate dynamic pressures (60 psf) even though five stages of reefing were employed. The severity of this problem was unexpected since drop tests and wind tunnel experiments with smaller parawings had indicated that with proper reefing, dynamic pressures at deployment of 100 psf were feasible (references 2, 3, and 4).

The general purpose of the present study is to determine the geometric, aerodynamic, and kinematic characteristics of the deployment phase of two of the flights, designated 203-T and 205-T, in which damage was experienced. A particular objective is to provide the data necessary for a structural analysis of one of the flights at the time of failure. For each flight, the results include the projected drag area of the canopy throughout all stages of deployment, the motion of various points on the canopy during inflation of the second, third, and fourth stages, and the canopy shape and pressure distribution at the critical times during first and second stage inflation. In addition, detailed canopy mold loft line drawings are presented for the critical (failure) time during second stage inflation of the flight (203-T) selected for subsequent structural analysis.

SYMBOLS

A	true projected length of an object as seen normal to the line of sight, in
a	reference point for wing cross section. Also, length of object of dimension A as measured on the film, in
afm	after first motion
alc	after line cut
C	wing chord, in. Also center wing (reefed) fore-aft dimension measured on the film, in
c	speed of sound, in/sec
CS	camera speed
c_p, ΔC_p	pressure coefficient and differential pressure coefficient, respectively
$C_D S$	drag area

C_xC, C_yC, C_zC	distributed load coefficients, chordwise, spanwise, and vertical
C_xS, C_yS, C_zS	total airforce coefficients, chordwise, spanwise, and vertical
D	slant range along the camera line of sight, in
d_R, d_L	translation of the right and left lobe axis with respect to the canopy axes, in., respectively
EAST, X, SOUTH, Y	horizontal range coordinates
$\vec{F}$	force vector on canopy surface, lb
F_{lc}, F_{lt}, F_{pcd}	number of camera frames to line cut of first stage disreef, line transfer, and program chute disconnect, respectively
F_x, F_y, F_z	x, y, and z components of $\vec{F}$, lb.
f	camera focal length, in
g/a	ground-to-air
$\vec{i}$, $\vec{j}$, $\vec{k}$	unit vectors directed along positive x, y, and z lobe axes
L	wing semispan. Also, true length from test vehicle center of gravity to the reference plane of the canopy, in
L.E.	wing leading or forward edge
L1, L2, ..., L6	leading edge suspension lines[1], left lobe, Figure 1
LK1, ..., LK12	keel suspension lines[1], left side, Figure 1
LT1, LT2, LT3	trailing edge suspension lines[1], left side, Figure 1
M	magnification factor for the motion analyzer
$\vec{n}$	unit vector, outward drawn normal to surface
p, p_s, Δp	pressure, static pressure, and differential pressure, lb/in^2
q	free stream dynamic pressure
R1, R2, ..., R6	leading edge suspension lines[1], right lobe, Figure 1
RK1, ..., RK12	keel suspension lines[1], right side, Figure 1
RT1, RT2, RT3	trailing edge suspension lines[1], right side, Figure 1

[1]Also used to denote the point at which the line is attached to the canopy.

r_x, r_y	parameters describing the chordwise and spanwise wing opening characteristics, Figures 9 and 10
$\dot{r}_x$, $\dot{r}_y$	dr_x/dt, dr_y/dt
$\ddot{r}_x$, $\ddot{r}_y$	$d\dot{r}_x/dt$, $d\dot{r}_y/dt$
r_{01} (t)	= L/SF = true length of vector $\vec{r}_{01}$ in the scale of the picture, in.
r_{01} (a)	projection of $\vec{r}_{01}$ in view (a), in.
S	projected wing area
SF	scale factor
t	elapsed time of flight, Table 1
t_{lc}, t_{lt}, t_{pcd}	time of line cut of first stage disreef, line transfer, and program chute disconnect
T.E.	wing trailing, or aft, edge
V	free stream velocity
ΔV	velocity change during arresting of inflation, ft/sec
v/a	vehicle to air
$\bar{x}$	maximum lobe half chord
x, y, z	lobe coordinate system, Figure 15
X, Y, Z	canopy coordinate system, Figure 15
x', y', z'	test vehicle coordinate system, Table 2
$\ddot{x}'$, $\ddot{y}'$, $\ddot{z}'$	components of test vehicle acceleration, Figures 5(a) and 6(a)
$\bar{z}'$	distance from test vehicle nose to center of mass, Table 2
Ix', Iy', Iz'	moments of inertia of the test vehicle with respect to its center of mass, about the x', y', z' axes respectively, Table 2
γ_F, γ_L	clockwise rotation of the right and left lobe coordinates with respect to the canopy axes, deg
η	dimensionless semispan coordinate
ψ, θ	transformation angles for computing true lengths from photographs (see Figure 21), deg
*	designates multiplication process (FORTRAN)

DESCRIPTION OF PARAWINGS AND FLIGHT TESTS

The flight data analyses described in this report are limited to the deployment phase of two drop tests, designated 203-T and 205-T, of the intermediate size, (4000 square feet), twin keel, parawing. These wings were developed under a NASA Langley Research Center contract with Northrup Ventura. The tests were conducted at the DOD Joint Parachute Test Facility, El Centro, California in October 1968.

Parawing Structure

The canopy structure and dimensions, together with the locations and extent of the failures, are shown in Figure 1. The canopies were fabricated from a low permeability (polyurethane coated) 2.25 oz/yd^2 nylon rip-stop fabric (MPDS 5-25.201). The typical panel width was 28.8 inches. Alternate panel seams were reinforced with nylon tapes (MIL-T-5608 - 1500 lb., 2000 lb., and 3000 lb., rated strength) sewn on both top and bottom surfaces. The locations of particular tape types is indicated by the total rated strengths shown in Figure 1. The keels and wing skirts were reinforced with nylon webbing (MIL-W-4088 - 3600 lb. bottom side and 5500 lb. top side for skirts; 9000 lb. for keels, 2 per keel). Nylon cords (MIL-C-7515 - 3500 lb., 4500 lb., 5500 lb., and 10,000 lb., rated strength) were used for the suspension lines. Leading edge suspension lines are designated L1, L2, ..., L6 and R1, ..., R6 for the left and right lobes respectively. All are 5500 lb. cords except for R3 and L3 which have a 10,000 lb. rating. Trailing edge suspension lines are designated LT1, LT2, LT3, and RT1, RT2, RT3, and all have a 3500 lb. rating. Keel suspension lines (12 each side) were attached at the intersection of the seam reinforcement and the keel webbing. All are 4500 lb. cords except for LK1, LK12, RK1, and RK12 which have a 5500 lb. rating.

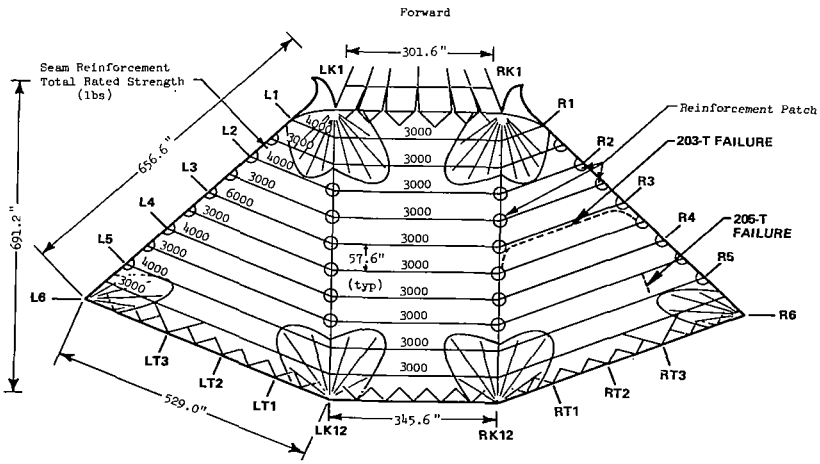

Figure 1. - Plan view of intermediate scale parawing.

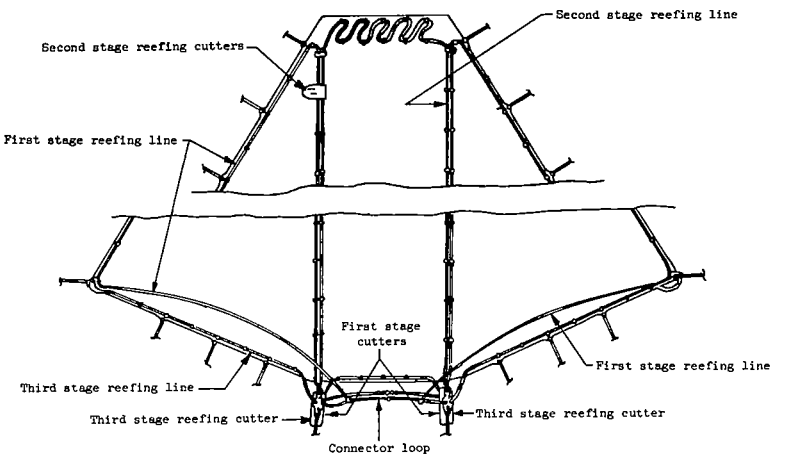

Figure 2. - Reefing diagram.

Deployment Technique and Reefing

In both flights the test vehicle was released from the test aircraft (C-119) at a velocity of 120 knots IAS and at an altitude of 20,000 feet. A program parachute stabilized the vehicle and brought the system to the desired level of dynamic pressure. At the proper time (preset) the program chute was released and the parawing pilot chute deployed. This chute extracted the parawing packing bag from the test vehicle and aided in its deployment. The deployment technique used in the tests consisted of five stages of disreef and inflation. The timing of each event is presented in Table 1. The reefing diagram is shown in Figure 2. The fully inflated shapes corresponding to the first four reefed stages are shown in Figure 3.

The parawing is extracted from the packing bag and deployed to the first reefed stage with all of the suspension lines of equal length. At the completion of first stage inflation, the reefing lines provide approximately the canopy shape shown for stage one. At this point all of the reefing lines are intact. Referring to Figure 2, the reefing lines pass through reefing rings which are attached to the canopy along the skirts and keels. In reefing, the canopy material between reefing rings is folded inward and the rings are brought together. The reefing line constrains the gathered assembly to a degree determined by the length of the line. The third stage reefing line constrains the trailing edge so that R6, RT3, RT2 and RT1 are gathered to RK12; RK12 and LK12 are brought together, and L6, LT3, LT2 and LT1 are gathered to LK12. The second stage reefing line gathers the keels and leading edge of the center lobe (i.e., points LK1, LK2, ..., LK12, and RK1, RK2, ..., RK12). Two first stage reefing lines are used, one for each side lobe. For the left side, the line is attached to LK12 and passes through loops along the reefed left keel to LK1, it then gathers the leading edge (i.e., points L1, L2, ..., L6), and terminates at the connector loop between the cutters at LK12 and RK12. The right side is of identical design.

The inflated stage one configuration, (Figure 3) consists of three air bags, each with its own inlet. The center lobe inlet lies at the geometric center of the lower surface and has a common segment (reefed keel line) with each side lobe inlet. The remaining segment of the side lobe inlet is formed by the reefed (side lobe) leading edge. The primary difference in the canopies of flights 203-T and 205-T is in the size of the inlets, which is determined by the lengths of the reefing lines. In particular, the center and side lobe inlets of 203-T had resultant reefed circumferences of 120.1 inches while 205-T had inlet circumferences of 86.4 inches. Since all of the suspension lines are of the same length at this time, all of the inlets should (approximately) be in a plane normal to the free stream flow and thus furnish ram air for inflation.

The first stage reefing lines are restrained at the wing tips (L6 and R6) by a connector loop which passes through eyelets at the ends of the lines. At first stage disreef, the restraint is removed by severing the connector loop at LK12 and RK12. The lines are subsequently drawn through the rings on the side lobe leading edges as the lobes deploy. At the completion of second stage inflation, the remaining reefing lines provide the canopy shape shown for stage two. The center lobe configuration is unchanged from stage one. The side lobes have a parachute - like configuration with the leading edge defining the parachute skirt.

At second stage disreef, the keels are released by cutting the second stage reefing line. The leading and trailing edge of the center lobe move apart with approximate symmetry until, at full inflation, the stage three configuration shown in Figure 3 is obtained.

At third stage disreef, the trailing edges are released by cutting the third stage reefing line. At full inflation after trailing edge deployment, the stage four configuration shown in Figure 3 is obtained. The final disreefing step (line transfer) consists of allowing the suspension lines to extend from equal lengths to their glide configuration.

Flight Data

The flight data included 16 mm color movie film, 70 mm black and white sequence photographs, telemetry records on test vehicle acceleration and suspension line loads, and Askania (space positioning and tracking) records.

The 16 mm color movie film were recorded by ground cameras, a camera on board the test vehicle, an air to air (chase plane) camera, and cameras on board the test aircraft. Nominal film speeds for the 16 mm ground cameras were 24 frames per second (40 inch focal length) and 100 frames per second (60 and 100 inch focal lengths). The airborne cameras had nominal speeds of 200 frames per second and the 70 mm ground camera was operated at a nominal speed of 10 frames per second. Unfortunately, locations of the ground cameras were not recorded.

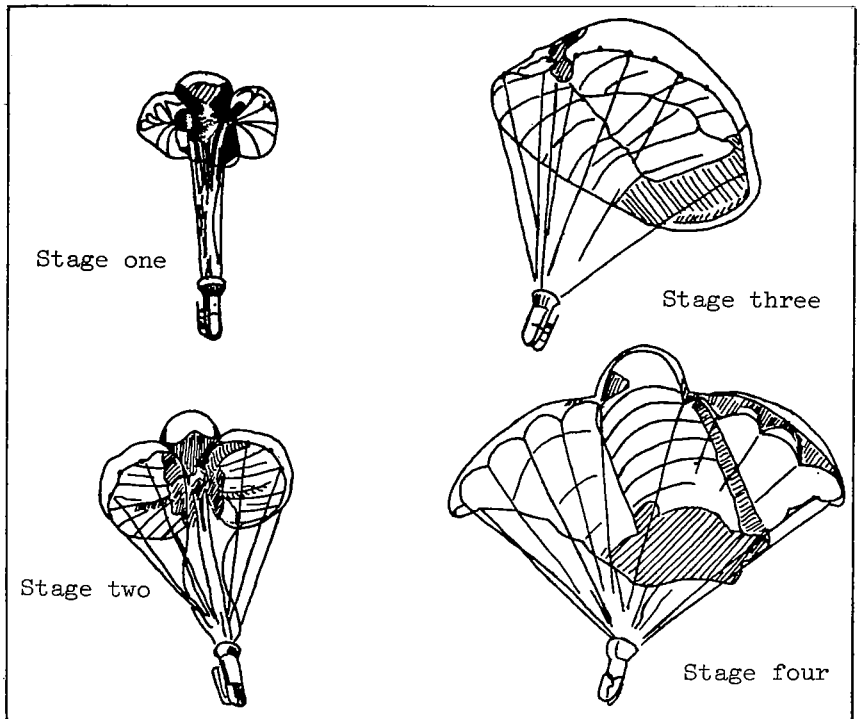

Figure 3.- Inflated conopy shapes.

TABLE 1 SEQUENCE OF EVENTS

No.	Event	Flight 203-T Elapsed Time-Sec	Flight 205-T Elapsed Time-Sec
1.	Time of launch flashbulb	0.048	-0.002
2.	Program chute inflation	3.549	3.110
3.	Program chute disconnect	27.357	26.246
4.	Line stretch	28.760	27.574
5.	First stage Parawing reefed inflation	29.596	28.537
6.	First stage reefing cut	35.063	33.956
7.	Second stage Parawing reefed inflation	35.354	34.559
8.	Second stage reefing cut	38.119	36.825
9.	Third stage Parawing reefed inflation	38.797	37.246
10.	Third stage reefing cut	41.581	40.634
11.	Line transfer	45.234	44.163
12.	Full Parawing inflation	46.748	45.618
13.	Landing impact	803.570	838.007

The dimensions and inertia data for the test vehicles are presented in Table 2. Except for the skids, the vehicles are geometrically symmetric about the z' axis. Two skids are permanently attached to the body of each vehicle with the skid runners parallel to the z' axis. The x' axis is chosen such that the skid runners are equidistant from the x', z' plane. The moments of inertia (Ix', Iy', Iz') are taken with respect to the center of mass (e.g., Ix' is the moment of inertia with respect to the center of mass about the x' axis).

The instrumentation layout is shown in Figure 4. Test vehicle acceleration was measured by a triaxial accelerometer located approximately at the vehicle center of mass. Suspension line loads were measured for lines LK12, L6, L3, and L1 (Figure 1) by load cells located 515 inches from the canopy skirt. Total suspension loads were taken from riser-vehicle links: forward and aft prior to line transfer; forward, aft, left, and right thereafter. The oscillograph records are shown in Figure 5 for flight 203-T and in Figure 6 for 205-T. The time, t, is the elapsed time in seconds as presented in Table 1. The events of Table 1 are indicated in Figures 5 and 6 by the numbered vertical lines. For example, the initial peaks shown in the forward and aft riser loads in Figure 5(c), occur at event 4, which according to Table 1 is line stretch. The vehicle accelerometer readings shown in Figures 5(a) and 6(a) refer to the x', y', z' vehicle coordinate system given in Table 2. For example, the $\ddot{z}'$ trace gives the acceleration in g's along the z' vehicle axis. In interpreting these data, it should be noted that while the null positions of the $\ddot{z}'$ and $\ddot{y}'$ traces are both 0.0 g's, the null position of the $\ddot{x}'$ trace is 1.0 g's. The reason for this is that the accelerometer traces were calibrated (nulled) with the test vehicle resting on its skids, so that in a free fall condition, the $\ddot{x}'$ trace will read 1.0 g's rather than 0.0 g's.

The Askania data were obtained from a cinetheodolite network of Askania and Contraves stations and include position, velocity, dynamic pressure, drag area, and parawing oscillation angle. The deployment histories of these data are shown in Figures 7 and 8. The time, t, is the elapsed time in seconds as introduced in Table 1. The position of the test vehicle parawing system is given in terms of its mean sea level altitude and its horizontal coordinates with respect to the range reference point. The East, X coordinate is measured along the East-West axis and increases in value to the East. The South, Y coordinate is measured along the North-South axis and increases in value to the South. The vertical coordinate with respect to the range reference point may be approximated by subtracting 13.0 ft. from the altitude. The parawing oscillation is defined by the angle off the vertical, which is measured from the vertical direction at the range reference point to the parawing axis connecting the test vehicle and the (assumed) centroid of the canopy. The drag area, C_DS, was calculated from the observed motion and dynamic pressure and refers to the entire canopy test vehicle system.

TABLE 2 TEST VEHICLE PROPERTIES

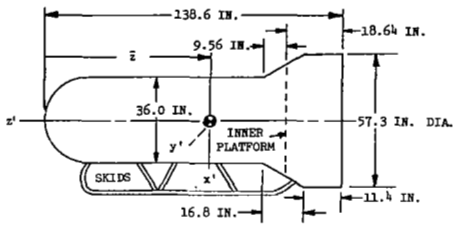

INERTIA DATA

Flight No.	Weight (lbs)	$\bar{z}$ (in)	$I_{z'}$	$I_{y'}$ (Slug ft^2)	$I_{x'}$
203-T	3465	47.3	195.9	816.6	856.0
205-T	4643	48.5	222.2	894.3	897.0

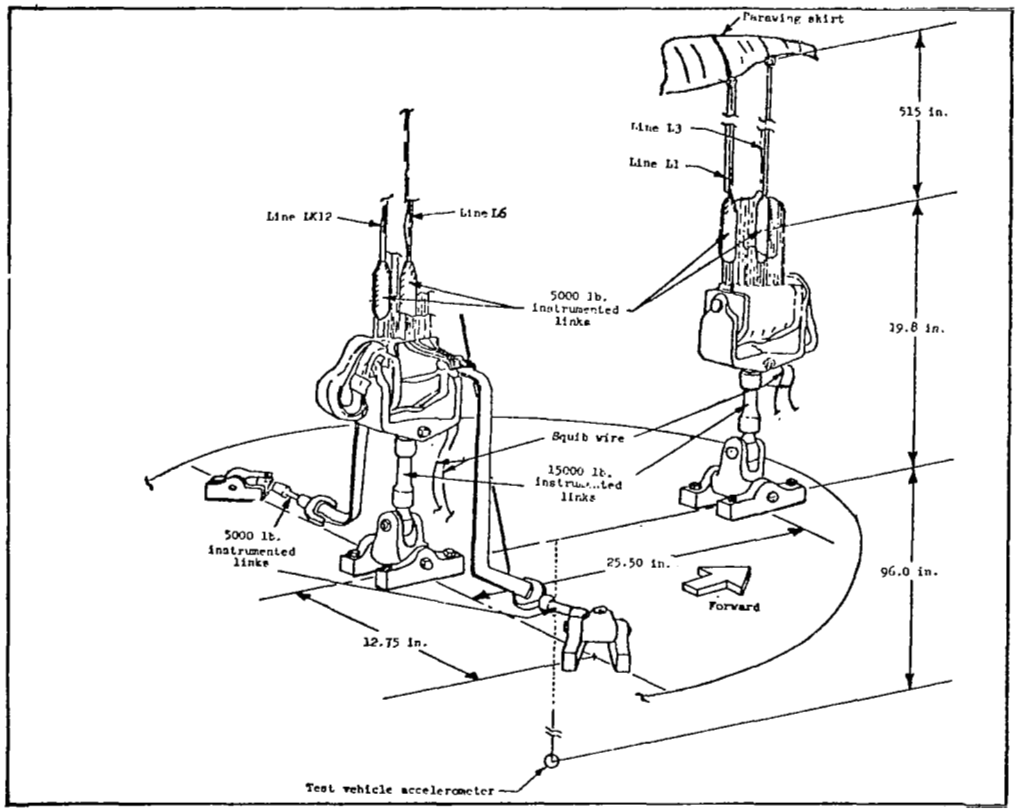

Figure 4. - Instrumentation layout

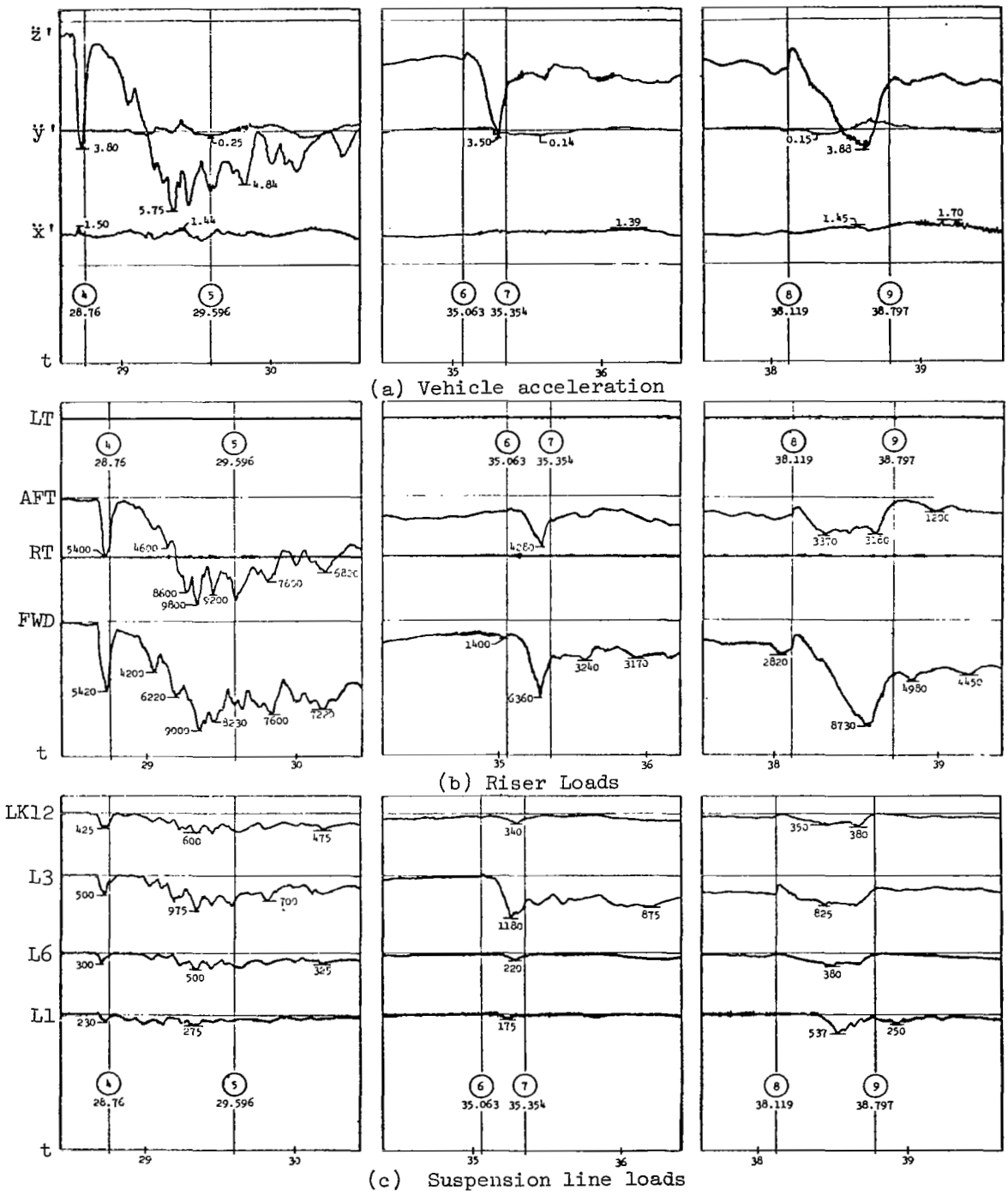

Figure 5. - 203-T Telemetry data

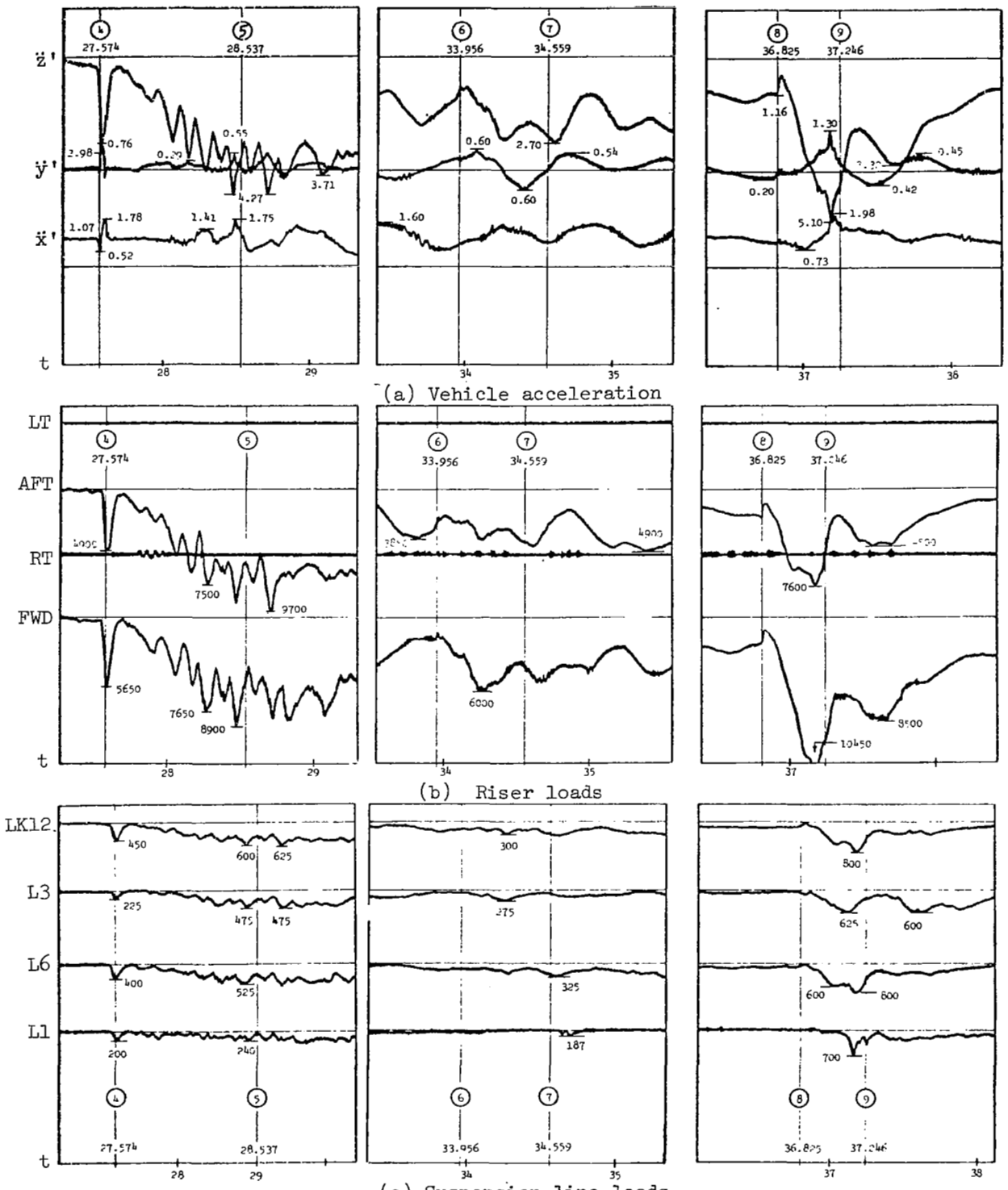

Figure 6. - 205-T Telemetry data

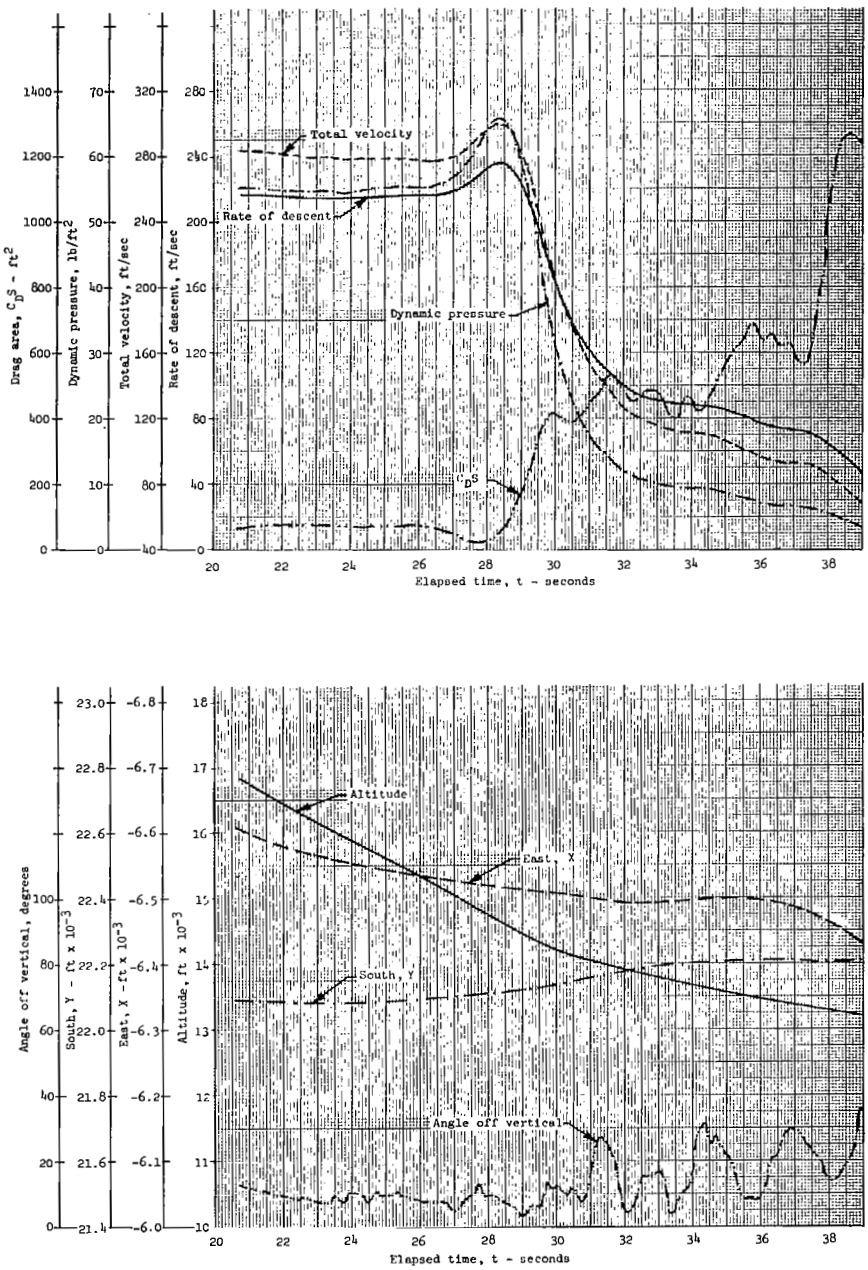

Figure 7. - 203-T Askania data

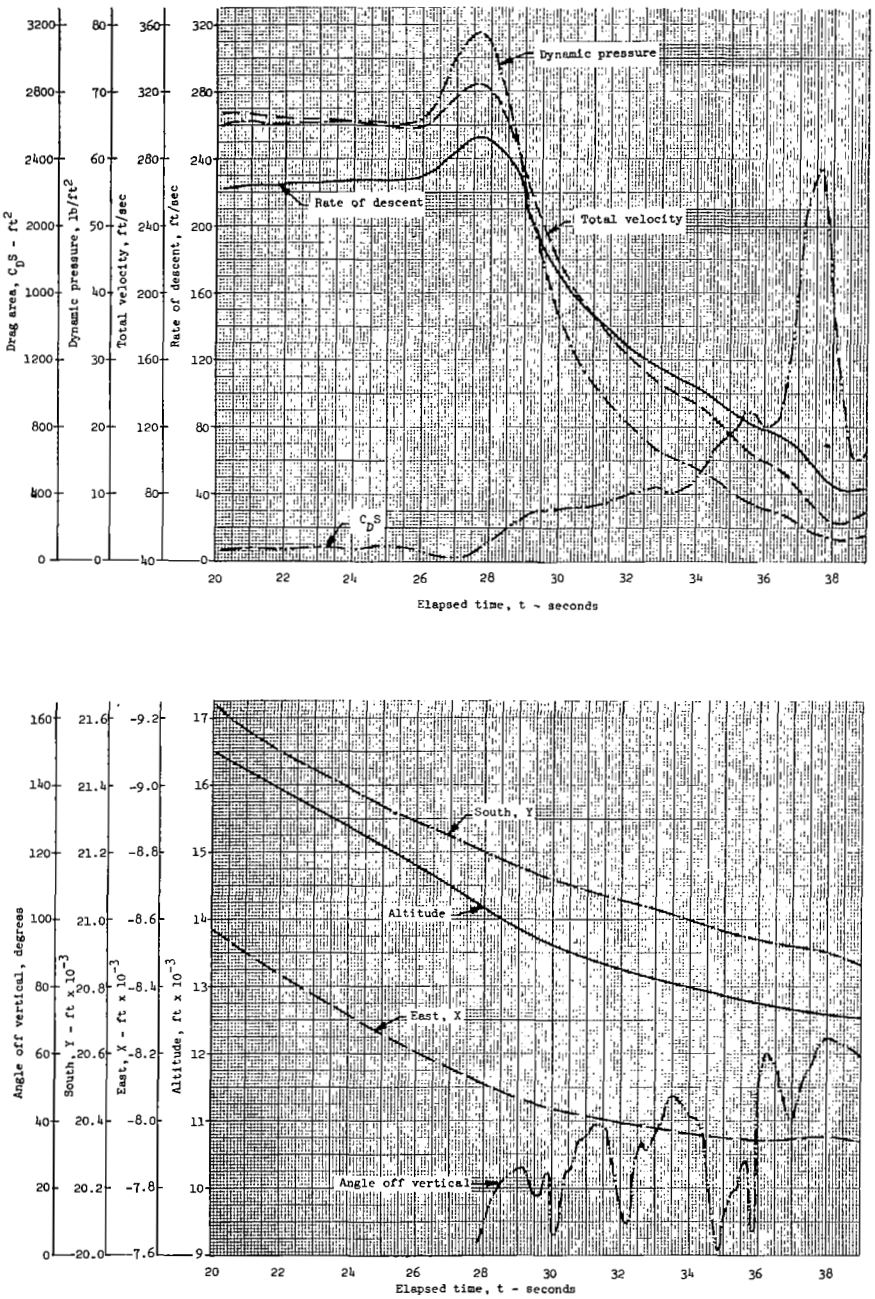

Figure 8. - 205-T Askania data

CANOPY MOTION AND AREA

The gross motion of both canopy test vehicle systems was given in the preceeding section by the Askania data (Figures 7 and 8). This section presents the time histories of the relative motion (displacement, velocity, and acceleration) of various points on the canopies during the critical deployment events from first stage disreef to line transfer. The displacement data were obtained directly from ground camera records. The velocity and acceleration were calculated by differentiation. In addition, the measured time history of the canopy projected drag area throughout deployment is presented for both flights.

Method of Analysis

A total of thirteen 16 mm color movie films were available for kinematic analysis of the two flights. Of these, only the ground to air cameras operating at 100 frames per second provided consistently usable data for canopy motion analysis. The test vehicle to air records could have been quite valuable except that the oscillation of the vehicle relative to the canopy frequently put the points of interest out of the field of view. Moreover, camera placement was such that the keel suspension lines obscured much of the right side of the canopy until after second stage disreef. The ground to air sequences at 24 frames per second were not used because of the slow frame speed. The primary difficulty with the air to air deployment records was that they were taken from a fixed wing aircraft maneuvering below the parawing - thus covering essentially the same area as the ground to air camera, but from a continuously changing view angle. Although the motion of the aircraft creates several problems in the development of detailed time histories, the air to air records would have been valuable (particularly in the development of instantaneous canopy shapes) had the aircraft been flying above the parawing.

The points selected for the study of canopy motion were chosen on the basis of their visibility in the film records and their ability to characterize the particular stage of inflation under analysis. From first disreef to line transfer, the only representative points whose motion could be consistently identified were the reinforcement patches on the leading edges (Figure 1). Similar patches on the keels were visible after second stage disreef. There were no characteristic identifiable points visible during first stage inflation and consequently no time histories were obtained for this stage. However, the motion during first stage inflation is discussed qualitatively in connection with the analysis to determine the peak loading conditions.

The relative displacements of points on the inflating canopy were obtained by means of overlays of the history of the canopy configuration during the stage considered. The overlays were traced from page size (8 x 10) images of the 16mm film projected on the working surface of a visual motion analyser. Reference points for overlay superposition were

selected on the basis of their stationary character. For example, during second stage inflation the shape of the center lobe remains essentially unaltered. Consequently, the outline of the inflated lobe and the position of its inlet were used for successive image orientation. In addition to the problem of selecting reference points, there are possibilities for errors in scaling, in timing, and in image shortening due to camera view angle. An assessment of the extent of these errors is presented in the Appendix, together with a detailed account of the motion analysis.

Results

The results of the relative motion analysis are presented in Figure 9 for flight 203-T and in Figure 10 for 205-T. For convenience two time scales are employed, the elapsed time of flight (Table 1) and the time after first motion. The latter is the time in seconds measured from the instant at which relative motion associated with a particular stage of inflation was first observed. The displacements shown represent basic data as measured directly from photographic images. Each figure includes a sketch of the characteristic view from which the data were derived, showing the dimension represented by the displacements. In addition, the applicable correction factor resulting from the consideration of error due to camera view angle is presented. To obtain corrected values, multiply the displacements, velocities, and accelerations given in the figures by the indicated correction factor.

The deployment of the right (or left) lobe during second stage inflation is characterized by two basic dimensions: The spanwise displacement of the attach point of suspension line R3 (or L3) relative to the centroid of the center lobe inlet, and the maximum chordwise dimension of the lobe inlet. The spanwise displacement data are presented in Figures 9(a), 9(b), 10(a) and 10(b). The chordwise inlet size data are shown in Figures 9(c) and 10(c). For second stage disreef to third stage inflation (Figures 9(d) and 10(d)), the dimension shown is one half of the displacement of a point on the leading edge relative to the center of the reefed trailing edge. Finally, fourth stage inflation (Figure 10(e)) is characterized by one half of the relative displacement of the attach points of suspension lines L6 and R6. At the completion of fourth stage inflation, this dimension is equal to one half of the parawing span.

The time histories of the projected drag areas of the two flights are shown in Figure 11. The areas were measured directly from the vehicle to air film and corrected to approximate normality with the flight path. The corrections were based on the Askania flight path data and the apparent angle between the camera line of sight and the suspension lines. The abscissa is the elapsed time in seconds as introduced in Table 1. The times at which the various reefing lines were cut are indicated in Figure 11 by the numbered vertical lines. The line numbers correspond to the event numbers of Table 1.

Discussion of Canopy Motion

Second stage inflation. - Second stage inflation is characterized by the motion of the leading edges of the side lobes. In the stage one configuration (Figure 3) the reefed side lobe leading edge forms part of the inlet for the lobe's air bag configuration. After the first stage reefing lines are freed by cutting the connector loop (Figure 2), the side lobe leading edges deploy to form the skirts of the parachute-like (stage two) lobe configuration shown in Figure 3. Unlike the axially symmetric opening of a parachute, however, the leading edge deployment is accompanied by distinctly different transverse (spanwise) and fore-aft (chordwise) motion. The spanwise motion is described by the displacement of attach points R3 and L3 relative to the centroid of the center lobe inlet (Figures 9(a), 9(b), 10(a) and 10(b)). The chordwise motion is described by the maximum chordwise dimensions of the lobe inlet as defined by the deploying leading edge (Figures 9(c) and 10(c)).

In flight 203-T, the first motion of the left lobe was observed immediately after the connector loop was severed. Motion of the right lobe was observed 0.03 seconds later, and the two lobes proceeded to inflate approximately simultaneously. At 0.21 seconds after the first motion was observed (afm), the spanwise displacement (Figures 9(a) and 9(b)) of points R3 and L3 reached the maximum allowed by the canopy geometry and the spanwise motion was suddenly arrested. Simultaneously, a tear failure was observed in the right lobe near point R3. The failure was apparently the result of the aerodynamic shock associated with the sudden termination of the spanwise motion. The tear propagated quite rapidly, so that after .08 seconds, it had extended over panel R3-R4-RK7-RK6 as shown in Figure 1.

The general character of the 203-T inflation is shown by the six views of Figure 12(a). In particular the symmetry up to the time of the failure is evident, as is the progression of the failure. The terminal spanwise velocities of both R3 (62 fps) and L3 (35 fps) were arrested within the time interval (0.01 seconds) between photographic frames. For this reason only lower bounds can be given for the impulsive decelerations. These estimates are: 193 g's for R3 and 109 g's for L3. As shown in Figure 9(a) the motion of point L3 was smooth, with a steady increase in velocity to a peak at .07 seconds afm followed by a gradual decrease to the terminal velocity of 35 fps at .21 seconds afm. This indicates that the left lobe reefing line was drawn smoothly through the leading edge rings. In contrast, the erratic velocity trace shown in Figure 9(b) implies that the right lobe reefing line encountered substantial resistance on two separate occasions as it was drawn through the leading edge rings. In each case, the resistance was suddenly released. The sudden release could explain the high terminal velocity of point R3. That is, restraint could allow a pressure buildup within the lobe which would lead to a relatively large acceleration if the restraint were suddenly removed.

The chordwise displacement history for the left lobe of 203-T is shown in Figure 9(c). The asymmetric character of the skirt deployment is evident upon comparison of these results with Figure 9(a). Indeed,

at the time of maximum spanwise displacement, the chordwise displacement was only half completed. Moreover, the completion of the chordwise displacement was not accompanied by high terminal velocities and impulsive deceleration at the skirt even though the maximum fore-aft full span velocity was approximately 70 fps at 0.1 seconds afm.

In flight 205-T, first motion was identified by a spanwise displacement of the right lobe suspension lines at approximately 0.14 seconds after the connector loop was cut. It took 0.18 seconds to complete the spanwise displacements of each lobe compared to 0.21 seconds in flight 203-T. However, the mode of inflation was quite different as is clearly illustrated by comparing the sequences shown in Figures 12(a) and 12(b). In particular, the side lobes deployed with approximate symmetry in flight 203-T, while in flight 205-T, the spanwise displacement of point R3 was practically completed before point L3 began its motion (at 0.16 seconds afm).

The velocity traces of points R3 and L3 (Figures 10(a) and 10(b)) indicate that the spanwise deployment of both lobes was smooth in flight 205-T. In fact, the terminal velocity and hence the deceleration of both points was negligible even though the maximum spanwise velocities were relatively high - 90 fps for R3 and 105 fps for L3. The chordwise expansion (Figure 10(c)) was somewhat more erratic. The forward edges of the right and left skirts were fully extended at 0.12 seconds afm and 0.28 seconds afm, respectively. The unfurling of both rear skirts was completed at about 0.95 seconds afm, with the right side lagging the left by approximately .09 seconds. Thus, even though the left side started its deployment .16 seconds after the right side, it achieved full inflation .09 seconds sooner.

A rip 16 to 20 inches in length was visible in the right lobe of 205-T (Figure 1) at 2.27 seconds afm (36.37 seconds elapsed time). The time at which the rip occurred could not be determined visually. However, there appeared to be some relatively high impulsive velocity changes associated with reversals in the right lobe curvature near the skirt during fore-aft inflation. Indeed, a velocity change of at least 37 ft/sec between frames (.01 second) was observed at the failure point at 0.18 seconds afm. The unfavorable camera view angle precluded a more accurate determination of the velocity. Even so, this leads to a lower bound of 115 g's for the aft impulsive deceleration at the point of failure. Although such reversals also occurred in 203-T, they were not as severe due to the higher degree of inflation of the lobes at disreef (compare Figures 12(a) and 12(b)). The full inflation of the 205-T left lobe prior to deployment eliminated the problem.

Third stage inflation. - The second stage reefing line (Figure 2) gathers the keels and the center lobe leading edge to form 75% of the center lobe inlet in the stage one and stage two configurations (Figure 3). After this line is cut (second stage disreef), the leading and trailing edge of the center lobe move apart with approximate symmetry to form the stage three configuration shown in Figure 3. The motion is described by

the displacement at a point on the leading edge relative to the center of the reefed trailing edge (Figure 9(d) and 10(d)). First motion is assumed to be coincident with reefing line cut.

In flight 203-T (Figure 9(d)), the second stage reefing lines were cut at 38.12 seconds elapsed time. The right side did not fully inflate, compared to the left side, due to the void in the ripped panel. In order to compensate for this and to produce conservative (larger) estimates of the displacement in keeping with the usual expected inflation, the dimension $2r_x$ was measured from the center of the reefed trailing edge to the attach point of line LK-1 as shown in Figure 9(d) (rather than to the center of the leading edge as in Figure 10(d)). A central opening (center lobe inlet) of approximately 2.0 feet existed at the time of first visible motion. This opening expanded to a maximum of $2r_x = 37.4$ feet at approximately 0.60 seconds afm. The maximum velocity of approximately 35 fps was constant over the time span 0.12 to 0.45 seconds afm, and decreased to zero at approximately 0.60 seconds afm without impulsive deceleration.

In flight 205-T (Figure 10(d)), the second stage reefing lines were cut at 36.82 seconds elapsed time. In this case dimension $2r_x$ was measured from the center of the reefed trailing edge to the center of the center lobe leading edge. The maximum corrected displacement ($r_x = 24.4$ feet) occurred at approximately 0.45 seconds afm. The maximum velocity of approximately 72 fps was constant over the time span 0.12 to 0.38 seconds afm. Although the motion terminated without an impulsive deceleration, a peak deceleration of 40 g's was measured at approximately 0.41 seconds afm.

Fourth stage inflation. - The third stage reefing line constrains the parawing trailing edge. After this line is cut (third stage disreef), the trailing edges of the center and side lobes expand symmetrically to their stage four configuration shown in Figure 3. The motion is described by the relative displacement ($2r_y$) of points L6 and R6.

In flight 205-T (Figure 10(e)), the third stage reefing line cut occurred at 40.63 seconds elapsed time. The maximum displacement, $r_y = 36$ feet, occurred approximately 1.10 seconds later. (First motion is assumed to be coincident with reefing line cut.) Velocity peaks were reached at 0.05 seconds afm (85 fps) and 0.55 seconds afm (43 fps) after which the velocity decreased to zero at approximately 1.10 seconds afm without impulsive deceleration.

No attempt was made to reduce the 203-T data for fourth stage inflation because of the extent of the canopy damage.

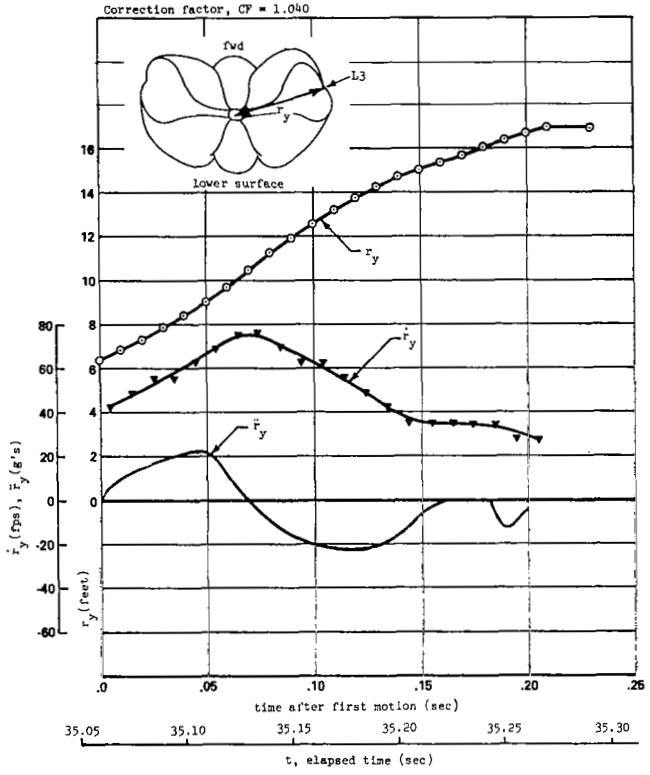

9(a) Spanwise displacement of point L3 relative to the centroid of the center lobe inlet during second stage inflation.

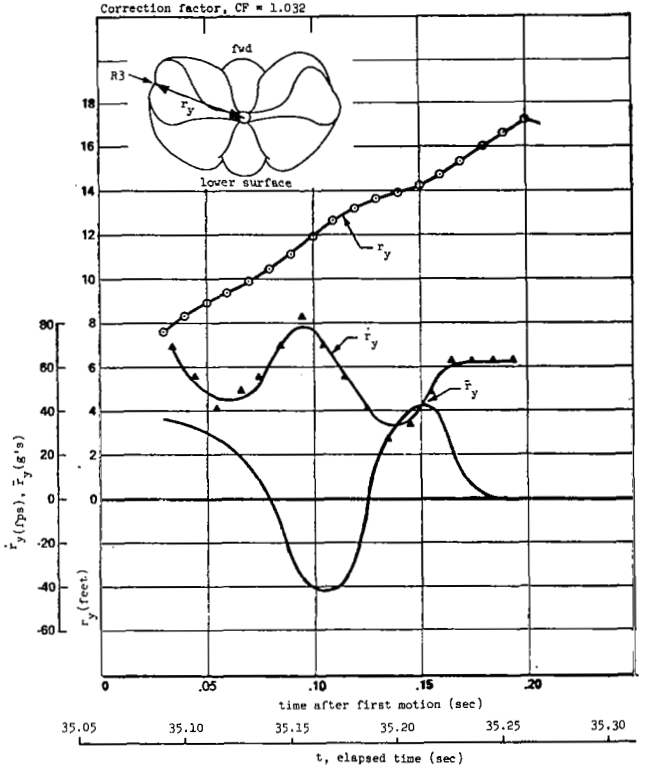

9(b) Spanwise displacements of point R3 relative to the centroid of the center lobe inlet during second stage inflation.

Figure 9. - Flight 203-T, relative motion of points on the canopy during deployment.

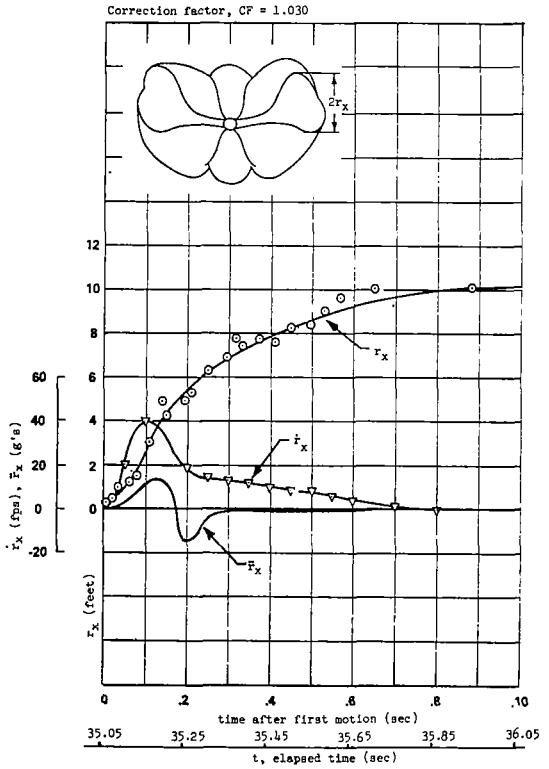

9(c) Chordwise expansion of the left lobe inlet during second stage inflation.

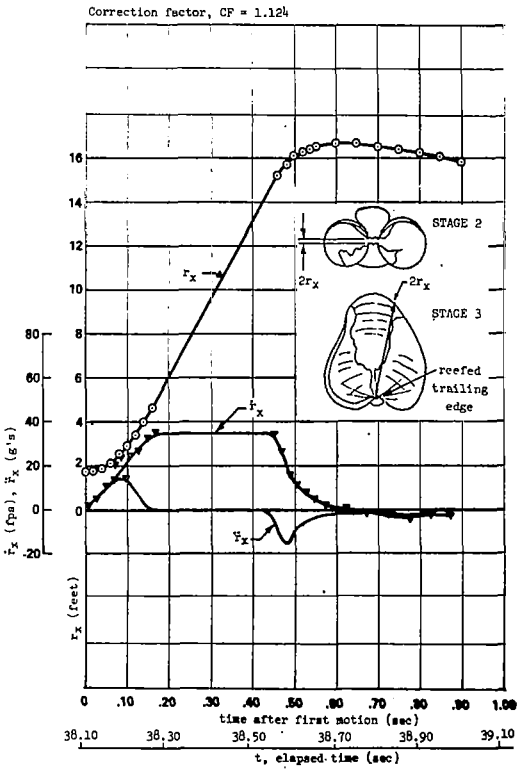

9(d) Chordwise expansion of the center lobe inlet during third stage inflation.

Figure 9. - Concluded.

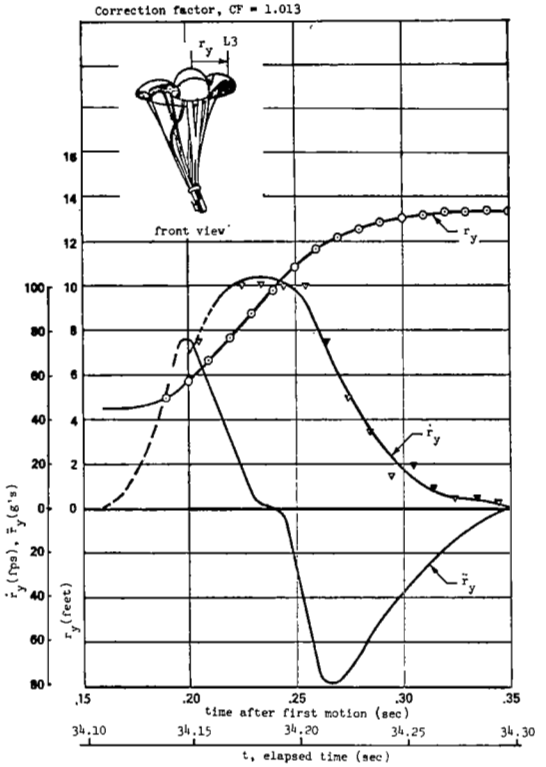

10(a) Spanwise displacement of point L3 relative to the centroid of the center lobe inlet during second stage inflation.

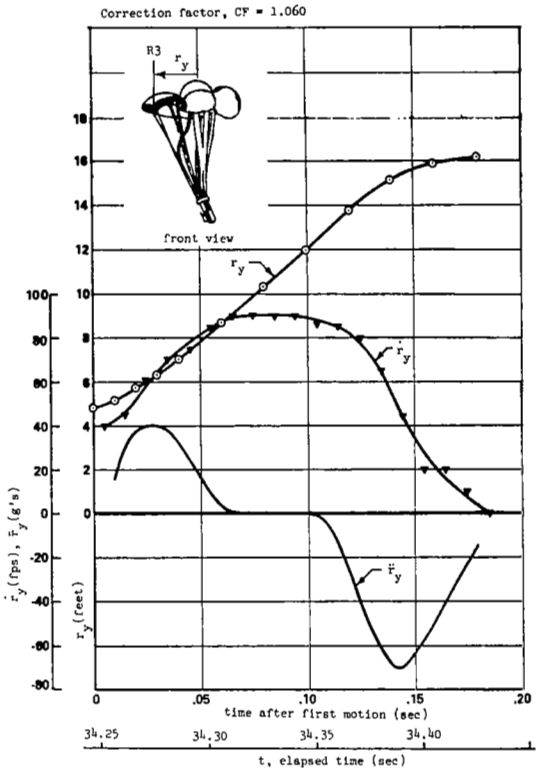

10(b) Spanwise displacement of point R3 relative to the centroid of the center lobe inlet during second stage inflation

Figure 10. - Flight 205-T, relative motion of points on the canopy during deployment.

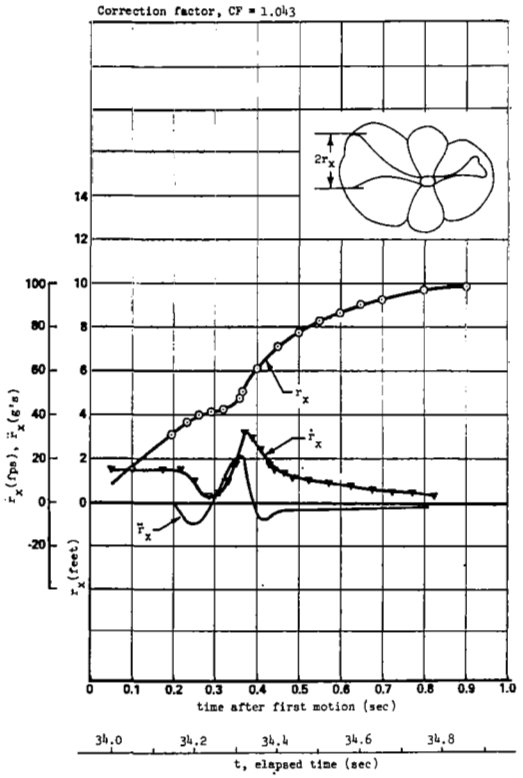

10(c) Chordwise expansion of the right lobe inlet during second stage inflation.

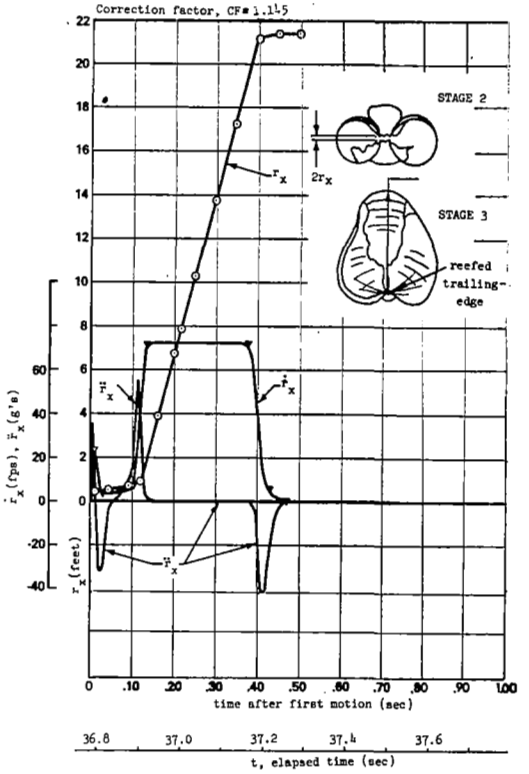

10(d) Chordwise expansion of the center lobe inlet during third stage inflation.

Figure 10. - Continued.

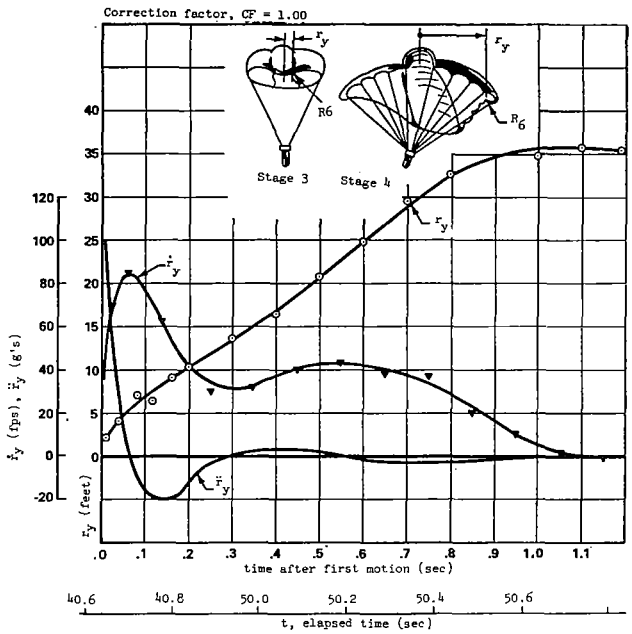

10(e) Spanwise displacement of point R6 relative to the center of the keel trailing edge during fourth stage inflation

Figure 10. - Concluded.

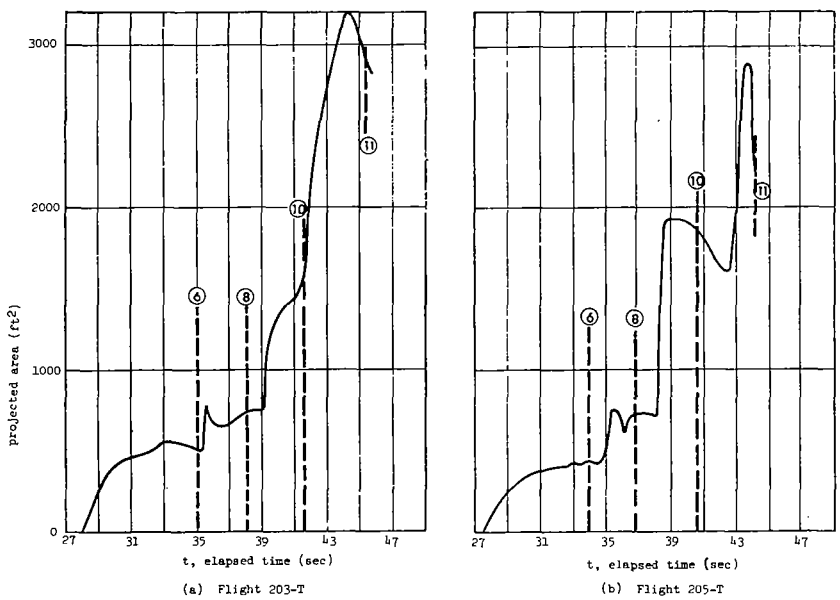

Figure 11. - Projected drag area.

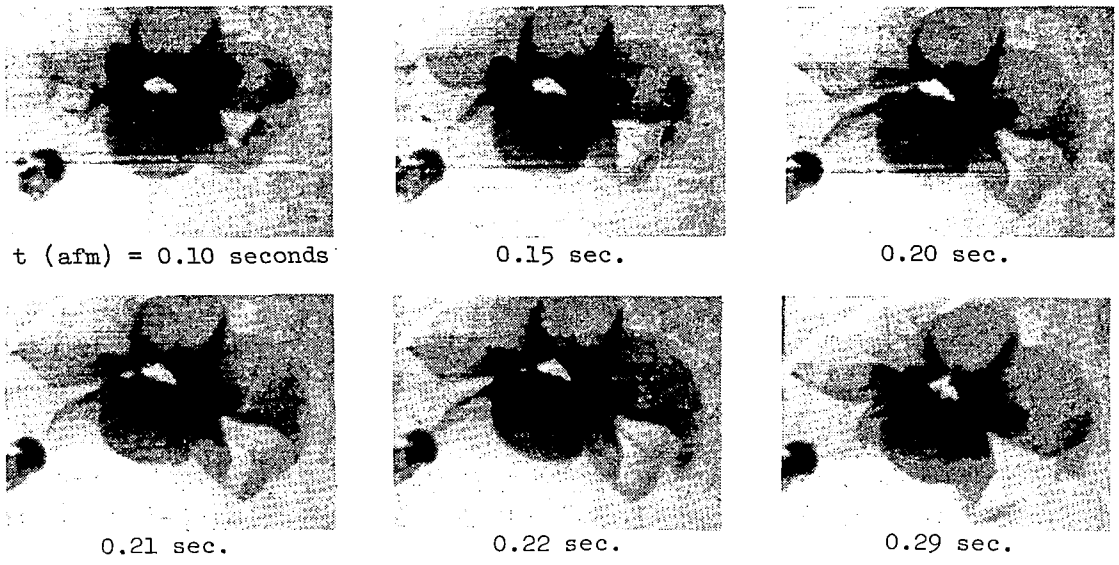

(a) Flight 203-T

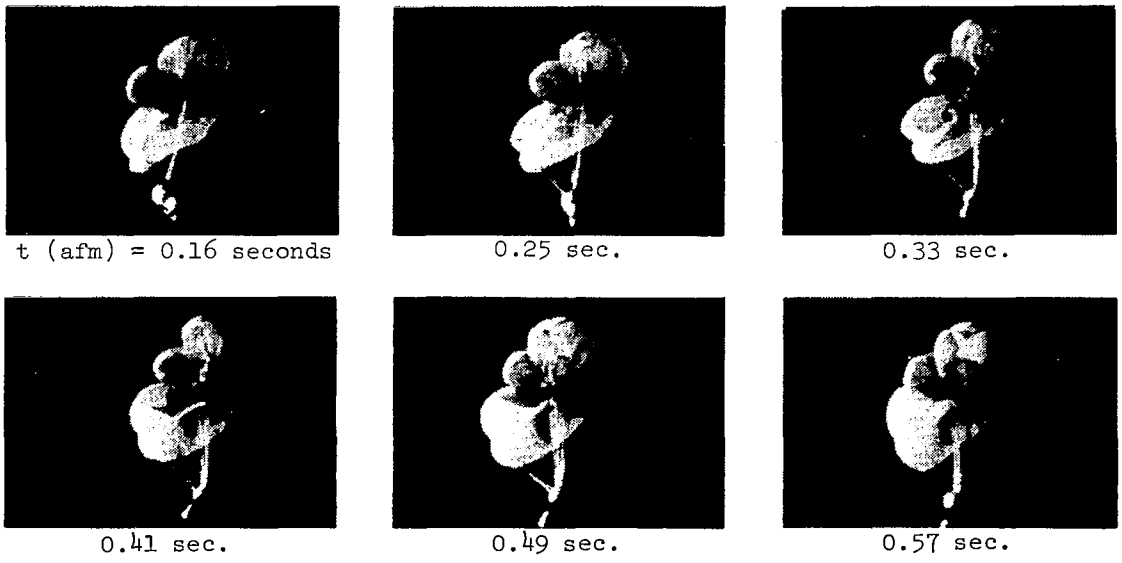

(b) Flight 205-T

Figure 12. - Second stage inflation

DETERMINATION OF CRITICAL LOAD CONDITIONS

The critical loading conditions occur prior to second stage disreef for tear failures of the right lobe were observed before this event in both flights. The critical times at second stage inflation, measured from first apparent motion after disreef, have been postulated based on visual evidence of severe opening shocks and (in the case of 203-T) canopy tear propagation. It remains, however, to correlate these postulated conditions with the suspension loads and to determine the critical time and conditions for the right lobe at first stage inflation. The resolution of these problems is attempted in the present section. In addition, a suspension load summary is presented for each stage of deployment.

The available loads data together with the instrumentation layout were presented (Tables 1 & 2 and Figures 4 through 6) in the general description of the drop tests. Since all the instrumented suspension lines were on the left side, the most important data for the present study are the test vehicle accelerometer and riser load traces.

First Stage Inflation

All reefing lines are intact during first stage inflation and the parawing configuration consists of three separate air bags, each with its own inlet (see Figures 2 and 3). Although the center lobe inlet can be observed throughout inflation, the side inlets, because of the dark background, are invisible until the leading edge moves laterally after the connector loop is severed (first stage disreef) as in the first frame of Figure 12(a).

First stage inflation begins immediately after line stretch when the pilot chute pulls away the packing bag. As can be seen from Figure 11, the average rate of inflation is quite slow compared to the later stages. This is also apparent in the accelerometer traces, (Figures 5 and 6) for the average slope of the $\ddot{z}'$ curve (prior to the peak value) is the same for both first and second inflation, but the average dynamic pressures are approximately 5 times as great at the first stage. Inflation continues for a considerable time after the peak deceleration. In flight 203-T it took 4.0 seconds to develop enough internal pressure to flatten the concave elements on the lower surfaces and form the fully inflated shape shown in the first frame of Figure 12(a). In 205-T, full first stage inflation was never completed. In general, the degree of inflation which can be accomplished in a given time depends upon the dynamic pressure and the inlet area. The average data for the two flights from line stretch to peak deceleration are presented in Table 3. The inlet area shown is the total of the three inlets as computed from the reefing line length, and the inflation rate is the average rate of increase of projected area.

Although the average rate of canopy inflation is slow, the presence of significant sawtooth fluctuations in the $\ddot{z}'$ trace (both before and after the peak value, Figure 5(a) and 6(a)), is indicative of rapid changes in

TABLE 3 FIRST STAGE INFLATION RATES

Flight No.	Inlet Area (sq. ft)	Dynamic Press.(PSF)	Inflation Rate (sq.ft/sec)
203-T	290	52	427
205-T	148	75	291

projected area about the mean. Consequently, the possibility of cyclic inflation-deflation (with accompanying shocks) of one or more lobes must be considered. To investigate this possibility, the photographic records were reviewed with the aim of correlating the motion and geometry of the canopy with the accelerometer readings. It was found that cycles of partial inflation and deflation of individual lobes were present and were accompanied by oscillations of the canopy as a whole. However, it was the behavior of the center lobe (and the corresponding canopy pitching oscillation) that appeared to be primarily responsible for the accelerometer fluctuations. This is illustrated in Figure 13 where a sequence of photographs in the neighborhood of the peak $\ddot{z}'$ trace of 203-T is shown. (This peak lasts from 29.33 to 29.36 seconds elapsed time, Figure 5(a)). At $t = 29.33$ and 29.58 the $\ddot{z}'$ trace was approaching maximum values and the center lobe appears to be fully inflated. At $t = 29.26$, 29.53 and 29.68, the $\ddot{z}'$ trace was near minimum values and the center lobe shows nominal inflation. The center lobe configuration also correlates with the $\ddot{z}'$ traces at the other times shown. At $t = 29.63$, the $\ddot{z}'$ trace had a peak (a continuation of the peak at $t = 29.58$) but the deceleration decreased sharply immediately thereafter. At $t = 29.47$, $\ddot{z}'$ was decreasing from a peak value at $t = 29.45$. Finally, at $t = 29.40$, a secondary peak occurred between the maximum at $t = 29.36$ and the minimum at $t = 29.43$.

No evidence of significant shock loading of the side lobes was observed in the film records. For this reason, it was assumed that the critical side lobe loading occurred as a static pressure coinciding with the $\ddot{z}'$ peak (nearest official first stage inflation) at which the maximum right lobe inflation was apparent. This assumption placed the critical times for first inflation at $t = 29.60$ seconds for 203-T and $t = 28.72$ seconds for 205-T. A summary of the suspension loads at the time of peak deceleration and critical right lobe loading are presented in Table 4.

Although the average rate of inflation of 205-T was considerably slower than for 203-T, the accelerometer trace fluctuations were much more pronounced. However, the snatch loads at the risers were unbalanced in this flight and the initial oscillation of the test vehicle resulting from this unbalance is thought to be partly responsible for the increased fluctuations.

TABLE 4 SUSPENSION LOAD SUMMARY FIRST STAGE INFLATION*

Event	Elapsed Time (sec.)	Suspension Line L1	L3	L6	Lk-12	Risers fwd	aft	Vehicle z'loading
203-T								
Initial spike	28.71	230	500	300	425	5420	5400	13,200
Maximum $\ddot{z}'$	29.35	275	975	500	600	9000	9800	19,900
Critical time	29.60	200	850	310	500	6700	8400	17,900
205-T								
Line stretch	27.57	200	225	400	450	5650	4900	13,800
Initial peak $\ddot{z}'$	28.47	240	475	525	600	8900	8450	19,800
Critical time	28.72	220	495	600	625	8350	9700	19,800

* All loads in pounds

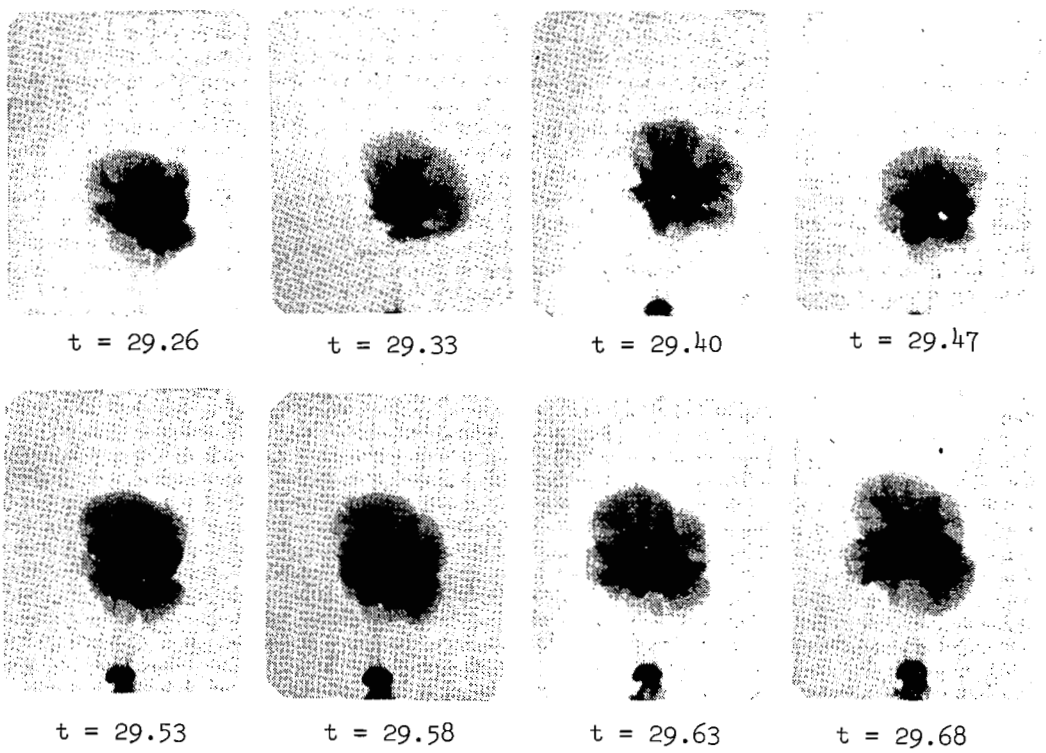

Figure 13. - Flight 203-T first stage inflation

Second Stage Inflation

In flight 203-T, the first stage reefing lines were cut at 35.06 seconds elapsed time. All major peak loads occurred from 0.20 to 0.22 seconds later (Figure 5). The peak vehicle deceleration, $\ddot{z}'$ = 3.5 g's, occurred at .22 seconds after line cut (alc) and was accompanied by $\ddot{x}'$ and $\ddot{y}'$ readings of 1.30 and 0.02 g's, respectively. Peak $\ddot{x}'$ and $\ddot{y}'$ readings were 1.35 and 0.18 g's, respectively at 0.20 seconds alc. In addition, discontinuities were observed in the $\ddot{z}'$ and riser load traces at this time, and the load in suspension line L3 reached a maximum value of 1180 lbs. The occurrence of the peak loading in line L3 places the completion of the transverse motion of the left lobe at 0.20 seconds alc. Since the motion analysis (Figure 9) showed that the transverse deployment of both lobes was completed at approximately the same time, 0.21 seconds afm, it appears that first motion and line cut coincide. Therefore, the loading conditions at 0.21 seconds alc represent critical conditions for the right lobe since the tearing was observed to begin at this time. It should be noted, however, that this does not eliminate the possibility that a small initial tear could have existed prior to line cut. A summary of the suspension loads for .20 and .21 seconds alc is presented in Table 5.

In flight 205-T, the first stage reefing lines were cut at 33.96 seconds elapsed time. There were two peaks in the vehicle z' axis accelerometer traces during inflation: $\ddot{z}'$ = 2.6 g's at 0.32 seconds alc and $\ddot{z}'$ = 2.7 g's at 0.68 seconds alc. Based on nominal camera speeds (as discussed in the Appendix), first motion of the right hand lobe occurred at 0.14 seconds alc. Therefore, (Figure 10), the first peak occurred at 0.18 seconds afm, coinciding with the completion of the transverse deployment of the right lobe, and the second peak occurred at 0.54 seconds afm, during the fore-aft inflation after deployment of the left lobe. The suspension loads occurring at these peaks are summarized in Table 5. The maximum riser loads also occurred at 0.18 seconds afm and were coincident with $\ddot{x}'$ = 1.6 g's (a peak) and $\ddot{y}'$ = 0.2 g's. Since the first peak is coincident with the completion of the transverse deployment of the right lobe, and the associated high local fore-aft canopy velocity transients noted in the previous section, the critical time for the right lobe is taken as 34.28 seconds.

Individual line loads measured on the left side developed only moderate levels in flight 205-T. In particular, the maximum load in line L3 was only 275 lbs, occurring at t = 34.28 seconds elapsed time, whereas in the 203-T flight this line load was 1180 lbs, more than 4 1/3 times as great.

Prior to 205-T first stage reefing line cut, the vehicle acceleration traces $\ddot{x}'$ and $\ddot{y}'$ were oscillating about their null positions (1.0g's and 0.0 g's) with amplitudes of 0.6 g's and 0.4 g's, respectively and a period of 0.85 seconds. The oscillation of the $\ddot{z}'$ trace was more complex. The fundamental period was 0.43 seconds and the maximum amplitude was 0.5 g's at 0.25 seconds prior to line cut. Evidence of "horizontal" loading during lobe deployment was apparent in the change in the character of the

TABLE 5 SUSPENSION LOAD SUMMARY SECOND STAGE INFLATION*

Event	Elapsed time (sec.)	Suspension Line L1	L3	L6	LK-12	Risers fwd	aft	Vehicle z' loading
203-T								
First peak	35.26	60	1180	176	210	6360	5750	12,127
						3820	2560	11,600
Critical time	35.27	- -	1080	220	300	5740	4280	12,000
205-T								
Critical time	34.28	- -	275	209	300	6000	4000	12,050
Second peak	34.64	187	116	375	327	5250	4520	12,500

* All loads in pounds

$\ddot{x}'$ and $\ddot{y}'$ oscillations (e.g., the $\ddot{y}'$ amplitude increases to .6 g's while the period decreases). However, the oscillations obscure a precise measure of the magnitude of the unequilibrated portion of the proposed fore-aft opening shocks in the right lobe at 0.18 seconds afm.

Third Stage Inflation

In flight 203-T, the vehicle deceleration $\ddot{z}'$ decreased 0.59 g's in the first 0.05 seconds after line cut (38.12 seconds elapsed time), and then increased steadily to a peak of $\ddot{z}'$ = 3.88 g's at 38.63 seconds elapsed time. The $\ddot{x}'$ and $\ddot{y}'$ components registered 1.45 g's and 0.15 g's coincident with the $\ddot{z}'$ peak. The corresponding forward and aft riser peak loads were 8730 lbs and 3180 lbs, respectively.

In flight 205-T, the vehicle deceleration $\ddot{z}'$ decreased 0.62 g's during the first 0.04 seconds after line cut (36.82 seconds elapsed time) and then increased steadily to a peak of $\ddot{z}'$ = 5.10 g's at 37.18 seconds elapsed time. Simultaneously, transverse acceleration peaks of $\ddot{x}'$ = 1.98 g's and $\ddot{y}'$ = 1.3 g's were recorded and the forward and aft riser loads were 10,000 and 7600 lbs, respectively. A summary of the suspension loads at the peak conditions for both flights is presented in Table 6.

TABLE 6 SUSPENSION LOAD SUMMARY THIRD STAGE INFLATION*

Event	Elapsed time (sec.)	Suspension Line L1	L3	L6	LK-12	Risers fwd	aft	Vehicle z' loading
203-T Peak	38.63	280	820	300	300	8730	3180	13,000
205-T Peak	37.18	700	625	800	800	10000	7600	23,600

* All loads in pounds

Fourth Stage Inflation

In flight 203-T, the maximum vehicle deceleration, $\ddot{z}'$ = 1.90 g's, occurred at 42.10 seconds elapsed time (0.52 seconds alc). The coincident transverse accelerations were $\ddot{x}'$ = 1.35 g's and $\ddot{y}'$ = 0.10 g's, and the forward and aft riser loads were 2600 and 2800 lbs, respectively.

In flight 205-T, the maximum vehicle deceleration, $\ddot{z}'$ = 1.75 g's, occurred at 41.10 seconds elapsed time (0.47 seconds alc). The coincident transverse accelerations were $\ddot{x}'$ = 1.28 g's and $\ddot{y}'$ = 0.15 g's, and the forward and aft riser loads were 3450 and 3800 lbs, respectively.

Assuming that line cut and first motion are simultaneous, the occurrence of the peak vehicle deceleration ($\ddot{z}'$) in flight 205-T, is in good agreement with the displacement history shown in Figure 10(d). The suspension loads at the time of the peak $\ddot{z}'$ are summarized in Table 7 for both flights.

Line Transfer

The suspension load summary for line transfer is presented in Table 8. In flight 203-T, line transfer occurred at 45.23 seconds elapsed time; full inflation at 46.75 seconds. The vehicle deceleration peak was $\ddot{z}'$ = 4.75 g's, accompanied by a forward riser load approximately double that of the aft riser. The forward riser load was 52% of the total riser peak load. The newly activated riser load transducers (right and left) recorded 30% of the total first peak load of 16,170 lbs. Line L6 bore the maximum peak load, 139% of the line L3 load and 40% of the total peak load of 2640 lbs.

In flight 205-T, line transfer occurred at 44.16 seconds elapsed time; full parawing inflation at 45.61 seconds. The peak vehicle deceleration was $\ddot{z}'$ = 2.54 g's. The forward riser peak load was 132% of the aft riser load and 44% of the total riser peak load. The newly activated riser load transducers recorded 23% of the total peak load of 11,425 lbs. Line L6, among the individual lines, bore the maximum peak load, 200% of that of line L3 and 55% of the total peak load.

TABLE 7 SUSPENSION LOAD SUMMARY FOURTH STAGE INFLATION*

Event	Elapsed time (sec.)	Suspension Lines L1	L3	L6	LK-12	Risers fwd	aft	Vehicle z'loading
203-T peak $\ddot{z}'$	42.10	90	375	50	80	2600	2800	6,600
205-T peak $\ddot{z}'$	41.10	100	200	0	100	3450	3800	8,100

* All loads in pounds.

TABLE 8 SUSPENSION LOAD SUMMARY LINE TRANSFER*

Event	Elapsed time (sec.)	Suspension Line				Risers				Vehicle z'loading
		L1	L3	L6	LK-12	fwd	aft	right	left	
203-T										
Initial	45.22	50	90	75	75	2450	2300	- -	- -	3,820
Peak load	46.45	370	860	1200	210	8480	4370	1650	1670	18,150
205-T										
Initial	44.15	25	100	25	0	1875	1600	- -	- -	3,840
Peak load	44.35	0	500	1000	325	5000	3800	1525	1100	11,780

* All loads in pounds.

Summary

Although cycles of partial inflation and deflation of individual lobes were present during first stage inflation, no evidence of significant shock loading of the side lobes was observed. It is assumed, therefore, that the peak loading conditions during second stage inflation are responsible for the failures.

The peak suspension loads during second stage inflation of flight 203-T occurred at the same time (35.37 seconds elapsed time) the spanwise motions of points R3 and L3 were arrested (Figures 9(a) and 9(b)). Since the tear in the right lobe first appeared at this time, it is reasonable to assume that the associated loading conditions are critical for the right lobe. Evidence to support the existence of significant aerodynamic shock loading in the left lobe is furnished by the magnitude of the load in suspension line L3 (Table 5) at the instant the spanwise motion of point L3 was terminated (approximately 35.26 seconds elapsed time). The conditions should be even more severe on the right lobe since the terminal spanwise velocities were 62 fps for point R3 and only 35 fps for point L3.

The peak suspension loads during second stage inflation of flight 205-T were coincident (34.10 seconds elapsed time) with the termination of the spanwise motion of point R3 and the abrupt reversals of curvature in the right lobe near the point of failure. Although no clear cut evidence was found in the telemetry data to substantiate the existence of severe aerodynamic shocks associated with the reversals in curvature, it is assumed on the strength of the visual evidence and the moderate character of the termination of the spanwise motion, that the fore-aft opening shocks exist and constitute the critical condition for the right lobe.

Because of the extent of the canopy failure, flight 203-T no longer represented the typical parawing during third inflation. On the other hand, the 205-T parawing with a relatively small 20-inch slit, was probably representative of the normal intermediate scale parawing with comparable payload. The difference in the canopies was evidenced by the reduced chordwise dimension (Figure 9(d)) of the 203-T parawing and its lower chordwise disreef velocity, $\dot{r}'_x$ = 35 fps vs. $\dot{r}'_x$ = 72 fps for the 205-T parawing. The higher vehicle deceleration $\ddot{z}'$ recorded for flight 205-T reflected the larger projected area (Figure 11) and a higher dynamic pressure. In both flights, the occurrence of the peak suspension loads coincides with the abrupt change in slope of the displacement histories (near maximum displacement) shown in Figures 9(d) and 10(d).

Fourth stage inflation and line transfer of flight 205-T were accomplished without impulsive or immoderate loads. Similarly, the suspension loads during fourth stage inflation of flight 203-T were moderate and indicated a deployment as smooth as that of flight 205-T. At line transfer,however, the peak axial deceleration of the test vehicle was quite large ($\ddot{z}'$ = 4.75 g's). This loading cannot be considered typical,however, because of the extensive canopy damage (a complete panel was useless for aerodynamic purposes at this time).

CANOPY GEOMETRY AND AERODYNAMIC PRESSURE DISTRIBUTIONS

This section presents the aerodynamic pressure distributions for the geometries of 203-T and 205-T at the selected critical times for the right and left lobes during the first and second stage inflations. The resultant aerodynamic loading (computed by integrating the pressure distributions over the canopy surface) is compared with the loading implied by the test vehicle accelerometer readings. As a prerequisite to the aerodynamic analysis, canopy geometry was developed at the critical times for each flight. In addition, detailed mold loft line drawings suitable for use in a canopy structural analysis were prepared for the critical time of 203-T second stage inflation.

Canopy Shapes

The canopy shapes were developed primarily from the ground camera records. As mentioned earlier, air to air records were available, but the aircraft was maneuvering below the canopy at the times of interest and the views were essentially the same as those obtained from the ground cameras. In particular, the upper surfaces of the canopy were hidden from all cameras by the lower surfaces at the critical times of first and second stage inflation. Therefore, the photographic data were insufficient to develop the cross sectional depth or the locations on the upper surfaces of the reinforcement tapes. For these reasons, a 1/20 scale model was built to augment the photographic data. The model was reefed by rigging according to Figure 2, "inflated" with foam rubber, and the lower surfaces and sides made to conform with the shape evident from the photographs. The section depth and tape locations were then taken from the inflated model.

The model is shown in Figure 14 in the fully inflated first stage configuration and the critical configuration at the termination of spanwise lobe deployment during second stage inflation.

The mold loft line drawings for the critical time of 203-T second stage inflation (t = 35.27 seconds) are shown in Figure 15. A right handed canopy coordinate system is assumed with its origin at the centroid of the center lobe inlet. The vertical Z axis coincides with the average direction of the center lobe suspension lines and is positive downwards, that is, in the direction from the canopy to the test vehicle. The XY plane is normal to the Z axis. The X axis measures the forward-aft direction (positive forward) and the Y axis measures the left-right direction (positive right). Right and left are defined for an observer on the top surface of the center lobe looking forward.

Figure 15(a) shows a view of the lower surfaces of the entire canopy together with the configuration of the right lobe tapes. The x and y coordinate grid shown superimposed on the right lobe lies in the X Y plane (z = Z) and defines the chordwise and spanwise stations at which right lobe lines were obtained. The latter are shown as x and y sections in Figures 15(d) and 15(e), respectively. The points where the sections cross the reinforcement tapes are indicated by a small circle on the section together with an identifying tape number. The tape numbers follow the same convention as the suspension lines and their attach points (eg, referring to Figure 1, tape R3 connects suspension line attach points R3 and RK6, while tape R3 1/2 is the tape midway between R3 and R4). Developed views of the right lobe and tapes are shown in Figures 15(b) and 15(c). It should be noted that the upward view of Figure 15(a) is of different scale than the other views of Figure 15.

In processing the photographic data, sequences of thirty-five mm negatives were made from the 16 mm film to bracket the critical time. The enlarged (3" x 3") positive prints of these negatives, together with the 5" x 5" sequence stills (from the 70 mm camera), were used to establish

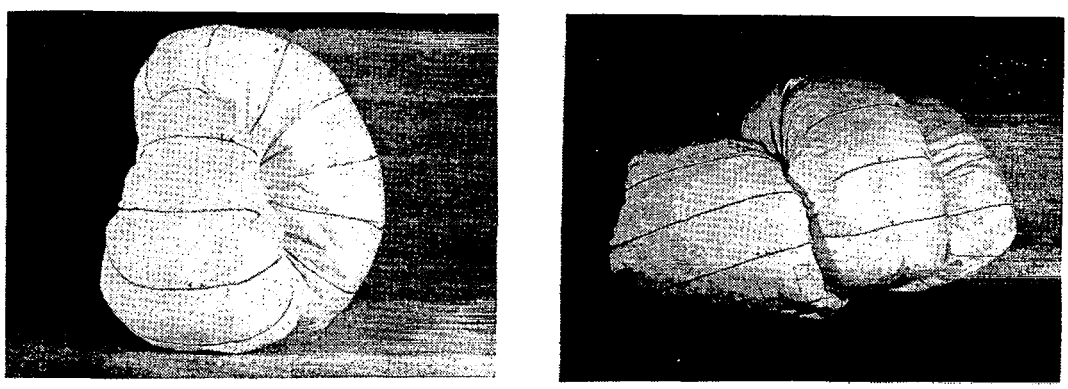

(a) First stage inflation (b) Second stage inflation

Figure 14. - Canopy Model.

the geometry of the lower surfaces and sides. Although the film coverage gave views of the inflation from the rear, left side, and (nearly) directly below, a precise perspective could not be determined - for the locations of the ground cameras and useful canopy direction cosines were not available. In addition, the only identifiable points on the side lobes were the reinforcement patches at the intersection of the reinforcement tapes and the leading edge. Consequently, the photographic data analysis was first concentrated on determining the x y z coordinates of the reinforcement patches and the overall projected dimensions of the lobes in each coordinate plane. The technique used to estimate the camera line of sight angle and the true lengths of dimensions measured on the photographs was similar to the procedure described in Appendix A. In addition to forming a basis for the mold loft lines, the results were used to establish geometric constraints for the model.

The side lobe openings of the model were constrained by wiring in a fiberboard insert cut to the dimension determined by the photographic analysis. The correct projected dimensions in the coordinate planes were obtained by the arrangement of the foam rubber inflating material. The center lobe inlet was constrained by the reefing line length. In regions of camera visibility, the model was used primarily to identify points. That is, with the aid of the model, a point selected in a view from the aft direction could be identified in a view from below. In other regions, measurements were taken directly from the model. In particular, most of the forward surface geometry and traces on the top surface of the reinforcement tapes were taken from the model. After correcting for camera line of sight, it is estimated that the error in relative positions of points determined by photographic analysis does not exceed $\pm$ 5%. The accuracy of the overall dimensioning depends upon the scale factor determination, which may be in error up to $\pm$ 16% (see Appendix A). Measurements taken from the model are as much as 10% too short due to its unstressed condition. The uncertain surface geometry in regions hidden from the cameras (i.e., geometry determined solely by the model) leads to an error estimate of $\pm$ 10% in the x y z coordinates of points on these surfaces. The effected region on the right lobe is that portion of the forward upper surface which is hidden from view in Figure 15(a).

In addition to the detailed structural drawing described above, canopy shapes suitable for the aerodynamic analysis were developed for both flights at the critical times of first and second stage inflation. The plan views and chordwise sections are shown in Figures 16 and 17 for flight 203-T and Figures 18 and 19 for flight 205-T. In each case, the chordwise sections are shown with the aerodynamic pressure distributions superimposed. The location of each section in the lobe coordinate system is defined by the coordinates (x_a, y_a, z_a) of the section reference point (a). These drawings were based primarily on the model and are consequently less accurate than Figure 15. The error in overall dimension due to scale factor determination is the same as before (up to $\pm$ 16%) and the additional error of $\pm$ 10% in the x y z coordinates due to scaling from the model must be applied to the entire surface.

t = 35.27 sec

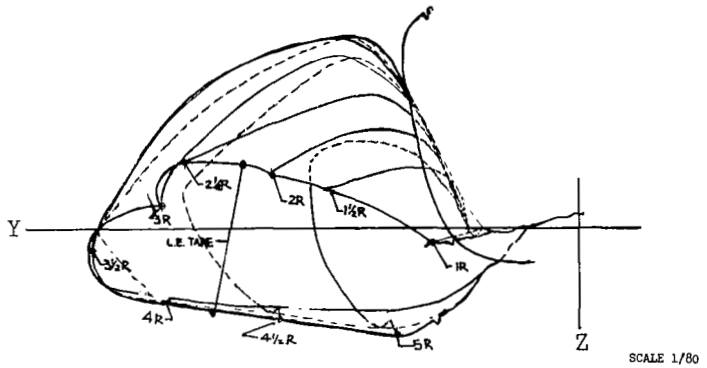

(b) Front view of right lobe

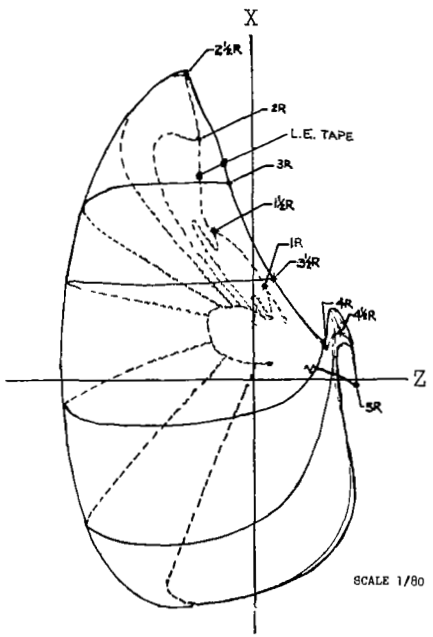

(c) Side view of right lobe

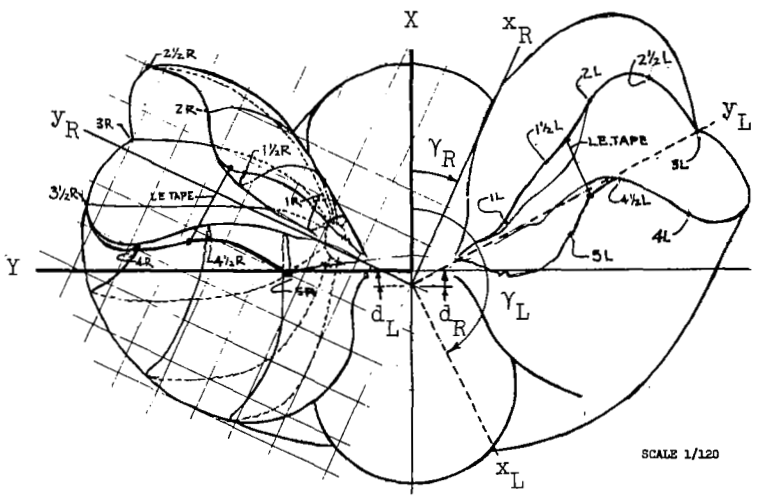

(a) View looking upward from risers

Figure 15. - Mold loft lines for critical time of 203-T second stage inflation.

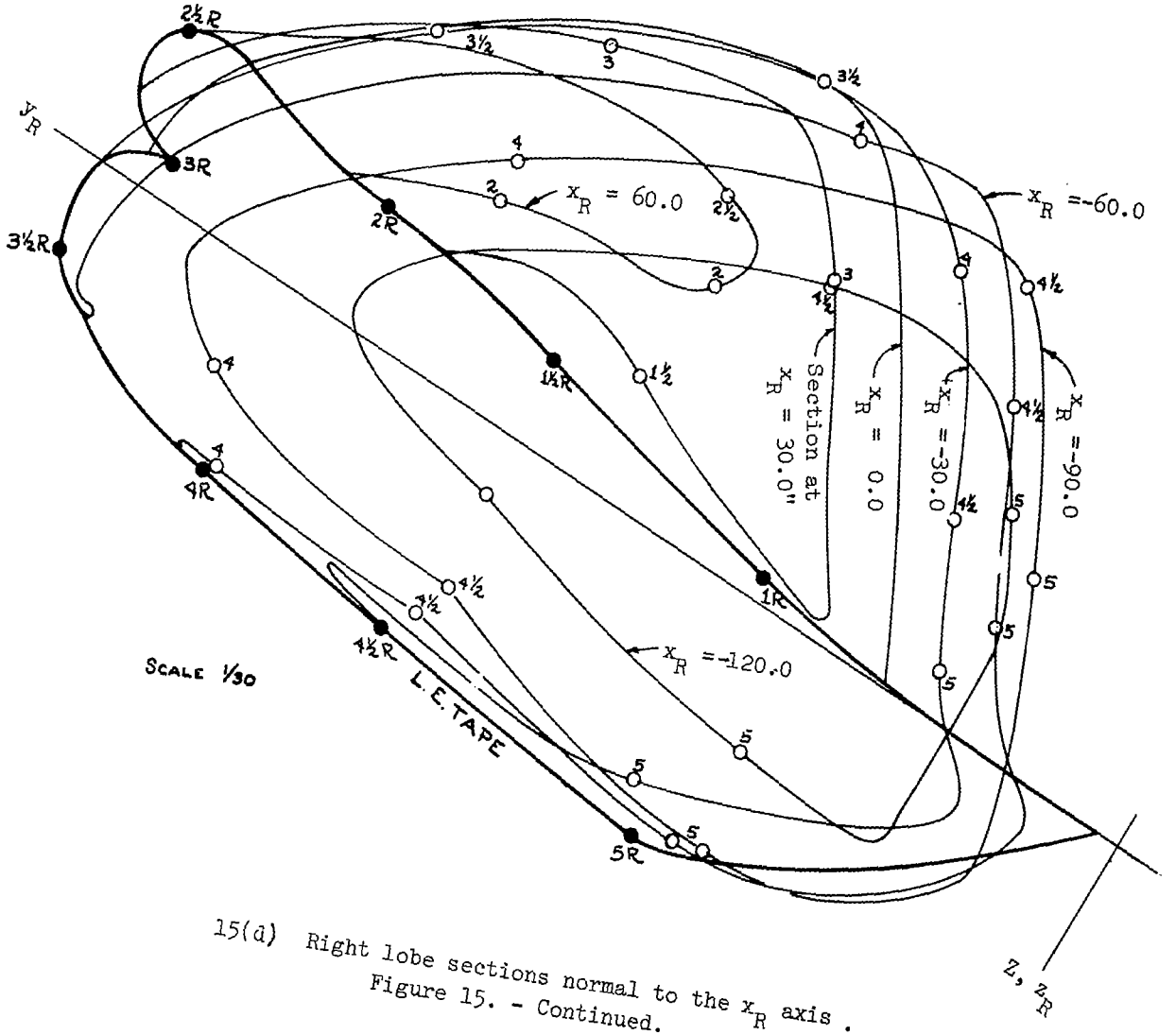

15(d) Right lobe sections normal to the x_R axis .

Figure 15. - Continued.

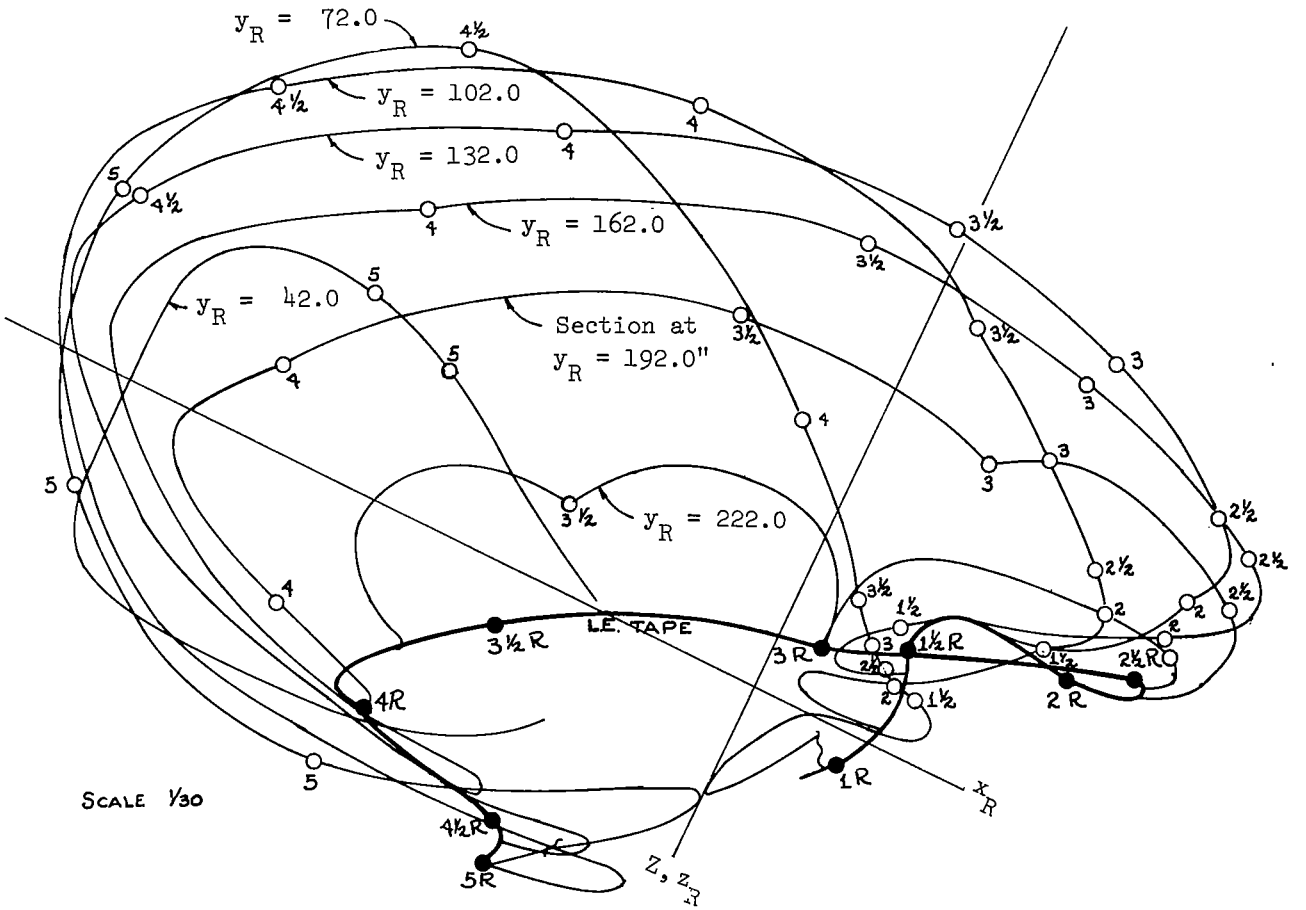

15(e) Right lobe sections normal to the y_R axis.

Figure 15. - Concluded

Aerodynamic Pressure Distributions

Internal and external aerodynamic pressure distributions were calculated for flights 203-T and 205-T at the critical times (for the right lobe) at first and second stage inflation. The critical times were selected in the preceeding data analysis as 29.60 and 35.27 seconds elapsed time for 203-T and as 28.72 and 34.28 seconds elapsed time for 205-T.

Method of Analysis - The pressure distributions were obtained by conventional approximation techniques combining closed form solutions, empirical results, and test data for similar conditions, and include contributions from potential flow, flow stagnation and separation, and shock waves. For a particular region, the choice of flow conditions was based on the configuration and motion of the surfaces and the loading conditions implied by the data analysis. In general, potential flow distributions were applied to all surfaces which were directly exposed to the free stream flow. Stagnation pressures were assumed to apply in trapped air regions and separated flow was assumed on the upper surfaces. In order to account for the apparent opening shocks, pressure pulse distributions were applied in regions of high canopy velocity transients at the critical time of second stage inflation. The effected regions were the right lobe of 205-T and both side lobes of flight 203-T.

The test data and procedure reported by Polhamus, Geller, and Grunwald (reference 5) for potential flow about non-circular cylinders formed the basis for the estimated static pressure distributions. The assumption is that flow about these non-circular cylinders would approximate that about applicable sections of the parawing. Indeed, the wide range of corner radii, Reynolds numbers and flow incidences tested permitted pressure estimates in separated flow regions as well as over surfaces directly exposed to the free stream flow.

The determination of pressure pulse distributions to represent the side lobe opening shocks was hindered by the scarcity of measured data - in fact, there were no opening shock pressure measurements available for the twin keel parawing. Recently however, Melzig and Schmidt (reference 6) were able to obtain internal, external and differential pressure distributions for parachute openings by means of small pressure transducers attached to the canopy surface. These tests were conducted under infinite mass conditions at wind tunnel speeds of 70, 100, 130, and 160 fps, and included four basic canopy types: solid cloth circular flat; solid cloth extended skirt; ring slot; and flat circular ribbon. As previously noted, the parawing lobe deployment is characterized by unsymmetric spanwise and chordwise motion, while parachute deployment is axially symmetric. Prior to the termination (critical time) of spanwise motion, however, the deployment of the outboard portion of the parawing lobe is kinematically similar to the later stages of inflation of the canopy models of the extended skirt type. It was assumed, therefore, that the outputs of the pressure transducers located at the test parachute skirt edge, apex, and two intermediate points are applicable to the outboard portion of the parawing lobes at the critical time.

In flight 203-T, the right lobe skirt edge velocities at the critical time were 60 fps spanwise and 40 fps chordwise, and the descent rate was 85 fps. This compares with terminal radial velocities at the test parachute skirt of 49 fps and 57 fps for wind tunnel speeds of 70 and 100 fps, respectively. The corresponding skirt edge differential pressure coefficients were 5.8 and 5.5 while at the apex the coefficients were 2.8 and 3.5. Because of the marked similarity in skirt edge velocity, it was decided to apply the test parachute results directly to the outboard portion of the right lobe. Following a conservative approach, the basic right lobe skirt edge pressure coefficient was taken from the 70 fps wind tunnel data while the apex and intermediate outboard pressure were based on the 100 fps test results. To account for the asymmetric opening geometry of the parawing side lobe, the center of total pressure pulse loading (apex) was assumed to be displaced in the outboard direction along the spanwise axis of the lobe to a point at 72.5% semispan (rather than 50% semispan for a symmetric opening). The pressure pulse distributions on inboard sections were obtained from the outboard distributions by assuming a carry over factor based on the section geometry and location relative to the apex.

The specific assumptions for the left lobe of 203-T center about the differences in terminal spanwise velocities at R3 and L3. As noted above, the terminal velocity of R3 was 60 fps and, from Figure 9(a), the terminal velocity of L3 was approximately 30 fps. Based on the assumption that the pressure pulse distribution can be scaled according to the incremental pulse relation $p = \rho c \Delta V$ (reference 7) the spanwise pressure pulse intensity at point L3 was reduced by a factor of two compared with the intensity at R3. The inboard pressure distribution of the right lobe was assumed to hold for the left lobe as well. The complete left lobe distribution was obtained by smoothing the skirt distribution associated with the motion of L3 into the basic inboard distribution.

In flight 205-T, pressure pulse distributions were considered for the right lobe only, which had an essentially free outboard inlet edge deployment similar to flight 203-T. The left lobe inlet was constrained, resulting in a gradual inflated deployment. The opening shock in the right lobe of 205-T is associated with an abrupt reversal of curvature of the aft skirt in the vicinity of the tear at 66.6 percent semispan. A terminal skirt velocity of at least 37 fps was associated with the reversal. Following the procedure used with the 203-T left lobe, the pressure pulse distribution was derived by scaling the outboard aft skirt edge coefficients to the 203-T coefficients at R3, based on the terminal velocity ratios, and then smoothing the resulting skirt distribution into the basic inboard distribution derived from the 100 fps test results of reference 6 (the descent rate for 205-T was 99 fps at the critical time).

Results - The results of the aerodynamic analysis are presented in Figures 16 and 17 for flight 203-T and in Figures 18 and 19 for flight 205-T. The data presented in Figures 16 and 18 pertain to the critical times of first stage reefed inflation and represent static aerodynamic conditions. Figures 17 and 19 present the results for the critical times

between first stage disreef and second stage inflation. The data shown for the right hand lobe in Figure 19 and for both side lobes in Figure 17 represent the parawing lobe-opening shock loading. The aerodynamic pressure coefficients are presented for chordwise cross sections at various positions of the dimensionless semispan coordinate η, where $\eta = 0$ bisects the center lobe and $\eta = 1.0$ is at the side lobe tip. Each figure also includes a sketch of the canopy configuration to which the distributions apply. In addition, plots of spanwise and chordwise running load distributions and total integrated loadings in the x, y, and z lobe directions are furnished.

The internal and external aerodynamic pressure distributions at a particular spanwise station, η, are represented by plots of the pressure coefficient, c_p, versus position on the chordwise canopy cross section at the station. In Figures 16 through 19, the value of c_p at a particular point is represented by the normal distance from the boundary of the cross section (solid line) to the boundary of the distribution (dashed line). A positive c_p is denoted by the arrow directed towards the surface, and a negative c_p is denoted by the arrow directed away from the surface. The appropriate scale factors are shown on the figures. The pressure, p, at a point is obtained from the scaled value of c_p by the usual relation

$$p = q\, c_p + p_s \tag{1}$$

where q is the dynamic pressure (which is also presented) and p_s is the static pressure at the test altitude.

Denoting a positive differential pressure, Δp, as acting outwardly on the canopy, then:

$$\Delta p = p_i - p_e \tag{2}$$

where the subscript i designates internal and the subscript e designates external. Substituting equation (1) into equation (2) and utilizing the subscripts for identification, then Δp is found to be independent of the static pressure and defined by

$$\Delta p = (c_{p_i} - c_{p_e})\, q = \Delta c_p\, q \tag{3}$$

It should be noted that although the full value of the pressure coefficient, c_p, is shown projected into the plane of the cross section, c_p actually refers to the normal to the canopy surface.

The force vector $\vec{F}$ due to the canopy pressures is defined by

$$\vec{F} = q \int_S \int \Delta c_p\, \vec{n}\, dS \tag{4}$$

where dS is the differential surface area whose outward drawn normal is defined by the unit vector, $\vec{n}$. If $\vec{i}$, $\vec{j}$, and $\vec{k}$ are unit vectors directed parallel to the x, y, and z lobe coordinates, respectively; then taking

the dot products of $\vec{F}$ with respect to $\vec{i}$, $\vec{j}$, and $\vec{k}$ yields

$$F_x = q \iint_{A_{yz}} \Delta c_p \, dy \, dz$$

$$F_y = q \iint_{A_{xz}} \Delta c_p \, dx \, dz \qquad (5)$$

$$F_z = q \iint_{A_{xy}} \Delta c_p \, dx \, dy$$

A_{yz}, A_{xz}, and A_{xy} are projections of the surface on the yz, xz, and xy planes, respectively. Since Δc_p is generally double valued (acts on two surfaces) for the coordinates yz, xz, and xy, it is necessary to perform the integration in two parts. Let:

$$C_xC = \int_{z_{min}}^{z_{max}} \Delta c_p \, (x, y_1, z) \, dz \qquad (6)$$

$$C_yC = \int_{z_{min}}^{z_{max}} \Delta c_p \, (x_1, y, z) \, dz \qquad (7)$$

$$C_zC = \int_{x_{min}}^{x_{max}} \Delta c_p \, (x, y_1, z) \, dx \qquad (8)$$

$\Delta c_p \, (x, y_1, z)$ is the differential pressure coefficient around the boundary of the curve f (x, z) for a chordwise cross section at y_1 parallel to the plane of the x z axes.

$\Delta c_p \, (x_1, y, z)$ is the differential pressure coefficient around the boundary of the curve f (y, z) for a spanwise cross section at x_1 parallel to the plane of the y z axes.

Substituting equations (6), (7) and (8) into equations(5) yields the orthogonal forces of the pressure loading in terms of the running load distributions and in the lobe coordinate system.

$$F_x = q \int_{y_{min}}^{y_{max}} C_xC \, dy \qquad (9)$$

$$F_y = q \int_{x_{min}}^{x_{max}} C_y C \, dx \tag{10}$$

$$F_z = q \int_{y_{min}}^{y_{max}} C_z C \, dy \tag{11}$$

The spanwise and chordwise airload distributions defined by equations (6), (7) and (8) were obtained by numerical integration for the various lobes and are furnished on Figures 16(b), 17(b) and (c), 18(b), and 19(b) and (c). The coefficients of the total airforce components in the lobe coordinates were obtained by integration of these distributions and are given on the figures.

The transformation of the aerodynamic force components from the lobe coordinate system to the canopy coordinates is accomplished by conventional matrix transformations. On Figure 15(a) the solid line coordinates for the right lobe are shown as x, y and z and are rotated clockwise through the angle γ with respect to the canopy axes. Letting the subscripts R and L be affixed to designate quantities associated with the right and left lobes, respectively; then the transformation of the lobe forces to the canopy system is accomplished by the following relationships.

$$\begin{Bmatrix} F_X \\ F_Y \\ F_Z \end{Bmatrix} = \begin{bmatrix} \cos\gamma_R & \sin\gamma_R & 0 \\ -\sin\gamma_R & \cos\gamma_R & 0 \\ 0 & 0 & 1 \end{bmatrix} \begin{Bmatrix} F_{x_R} \\ F_{y_R} \\ F_{z_R} \end{Bmatrix} + \begin{bmatrix} \cos\gamma_L & \sin\gamma_L & 0 \\ -\sin\gamma_L & \cos\gamma_L & 0 \\ 0 & 0 & 1 \end{bmatrix} \begin{Bmatrix} F_{x_L} \\ F_{y_L} \\ F_{z_L} \end{Bmatrix} \tag{12}$$

The values of γ_R and γ_L and the components of force in the canopy coordinate system are recorded in the following Table 9 for the main events of interest.

TABLE 9.- TOTAL AERODYNAMIC FORCES.

(a) 203-T

Event	Elapsed time, sec.	Axes Rotation		Total Aerodynamic Forces, Lb.		
		γ_R°	γ_L°	F_X	F_Y	F_Z
1st stage inflation	29.60	0	180	0	0	-17900
2nd stage inflation	35.27	25	153	330	1660	-12400

TABLE 9.- CONCLUDED.

(b) 205-T

Event	Elapsed time, sec.	Axes Rotation		Total Aerodynamic Forces, Lb.		
		γ_R°	γ_L°	F_X	F_Y	F_Z
1st stage inflation	28.72	0	180	0	0	-19800
2nd stage inflation	34.28	15	165	-1360	365	-13000

Discussion - The results shown in Table 9 and in Figures 16 and 18 represent the static aerodynamic conditions corresponding to the simultaneous occurrence, nearest official first stage inflation, of the peak vehicle axial ($\ddot{z}'$) accelerometer reading and the maximum right lobe inflation. The choice of this criteria was based on the absence of significant shock type loadings during inflation of the right lobe. The distributions were adjusted such that the integrated force, $q\ C_zS$, agreed with the vehicle axial deceleration. For 203-T, at 29.60 seconds elapsed time, the vehicle axial deceleration implied a drag loading of 17,900 lbs. For the measured dynamic pressure of 42.5 psf, this implies an effective drag area (C_DS) of 420 sq. ft. which agrees with the negative of the integral, C_zS, of the vertical (z) loading shown in Figure 16(b). Similarly, the vertical (z) loading shown for 205-T in Figure 18(b) agrees with the 317 sq. ft. effective drag area implied by the 19,800 lb vehicle inertia load and 62.5 psf dynamic pressure at 28.72 seconds elapsed time.

The results shown in Figures 17 and 19 coincide with the peak vehicle axial decelerations ($\ddot{z}'$) in the interval between first disreef and second inflation. The implied vehicle inertia loading was approximately 12,000 lbs. in both flights and the spanwise vertical load distributions shown are in agreement with this loading. The vertical load distributions for 203-T and the right lobe of 205-T show a large pressure pulse loading from $\eta = 0.5$ to $\eta = 1.0$, while the distribution shown for the 205-T left lobe represents static conditions.

The spanwise (y) lobe loadings for 203-T are shown in Figure 17(c). Although this loading is partially equilibrated, the differences in C_yC for the two lobes, when resolved for the lobe rotations and considering the "x" interactions, accounts for the major portion of the 1660 lb sideforce to the right shown as F_Y in Table 9(a). No attempt was made to adjust the distributions to enforce agreement of the overload with the x' and y' accelerometer readings since vehicle oscillation and the lack of directional reference impair the interpretation of the measurements. However, the 1660 lb overload compares favorably with the resultant x', y' inertia loading of approximately 1400 lbs.

The spanwise lobe distributions for the x coordinates as shown for 205-T (Figure 19(c)) arises from the chordwise opening shock associated with the sudden reversals in curvature of the aft (trailing) skirt of the right lobe from concave inward to convex. The extent of the reversals at the critical time is shown in the right lobe chordwise cross sections. The inflated (convex) skirts shown on the left lobe sections are the result of the delayed inlet edge deployment. The magnitudes of the x shock loading on the right lobe was estimated at -1450 lbs. The x loading on the left lobe was essentially zero. The resolved loading in the X canopy direction is -1360 lbs., given as F_X in Table 9(b) for t = 34.28 seconds.

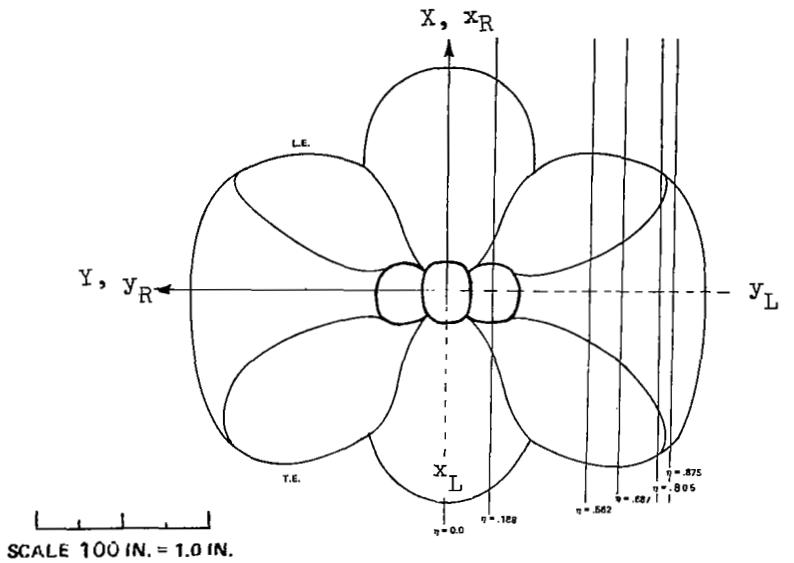

(a) Configuration, bottom view.

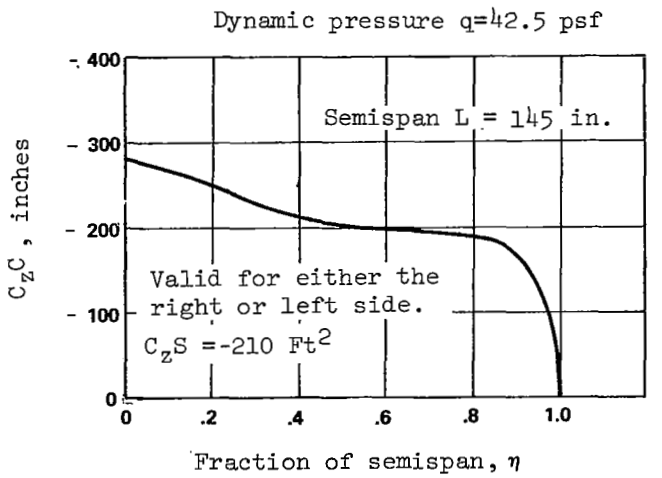

(b) Vertical (z) loading

Figure 16.- Aerodynamic loading for flight 203-T at first stage inflation, 29.60 seconds elapsed time.

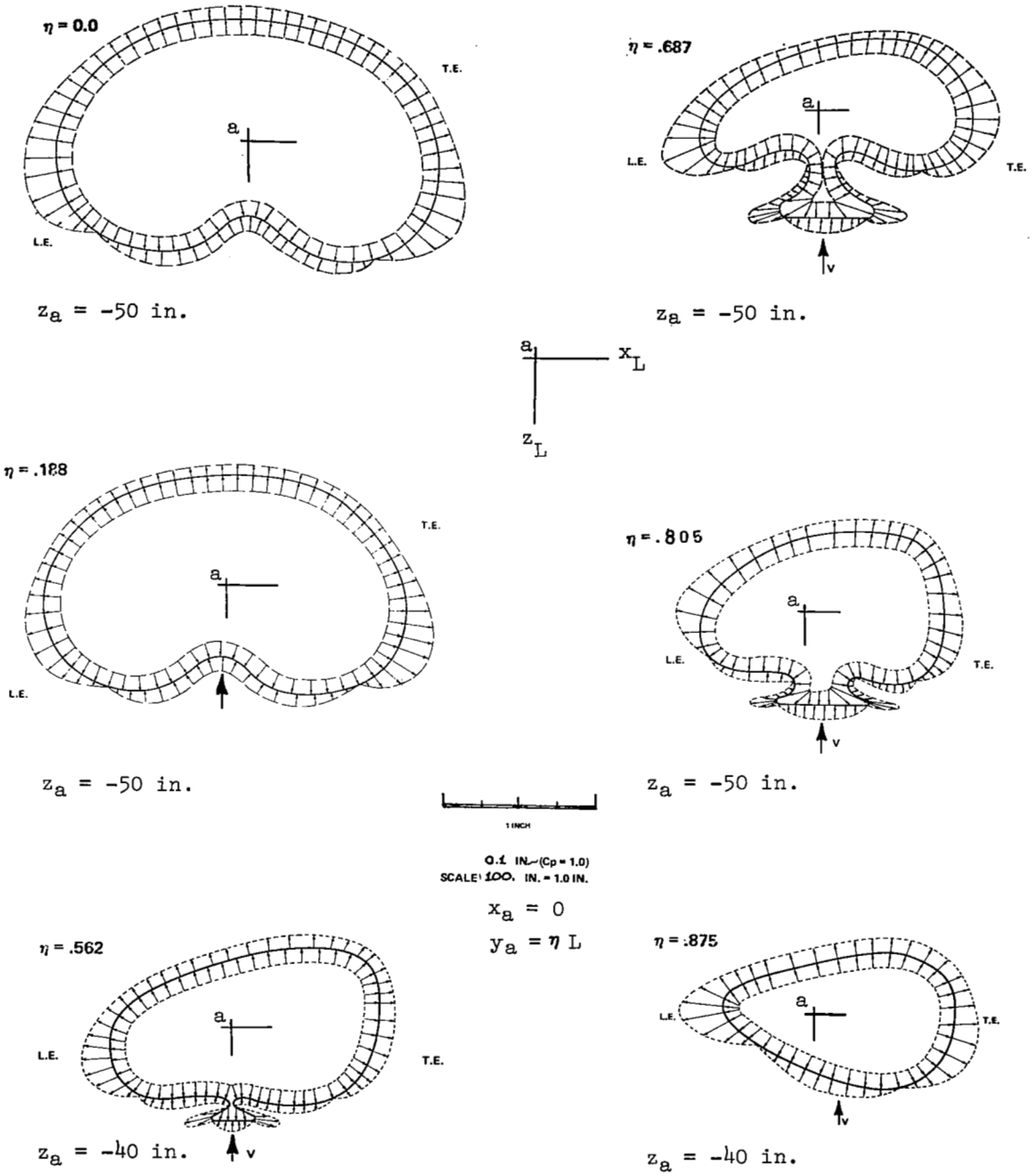

(c) Pressure distributions, left lobe (right lobe similar)

Figure 16.- Concluded.

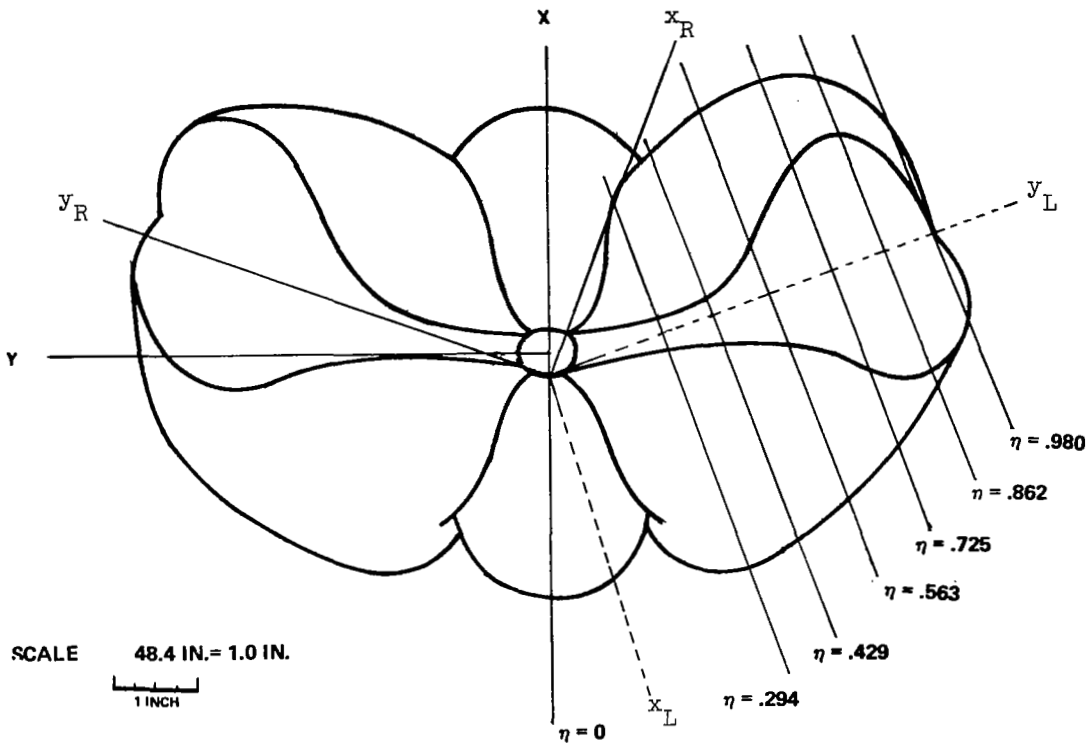

(a) Configuration, bottom view.

Dynamic pressure, q=8.0 psf

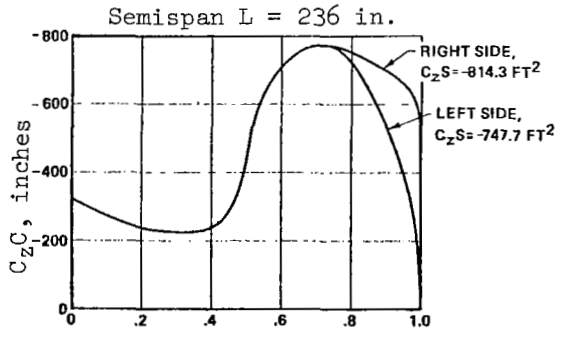

(b) Vertical (z) loading.

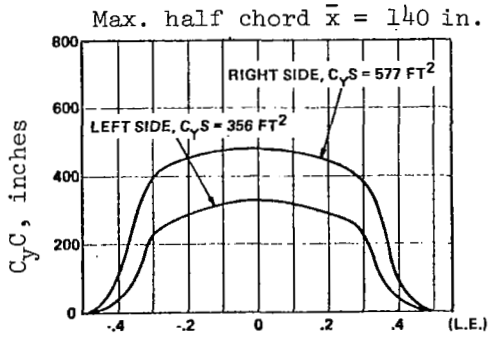

(c) Spanwise (y) loading.

Figure 17.- Aerodynamic loading for flight 203-T at second stage inflation, 35.27 seconds elapsed time.

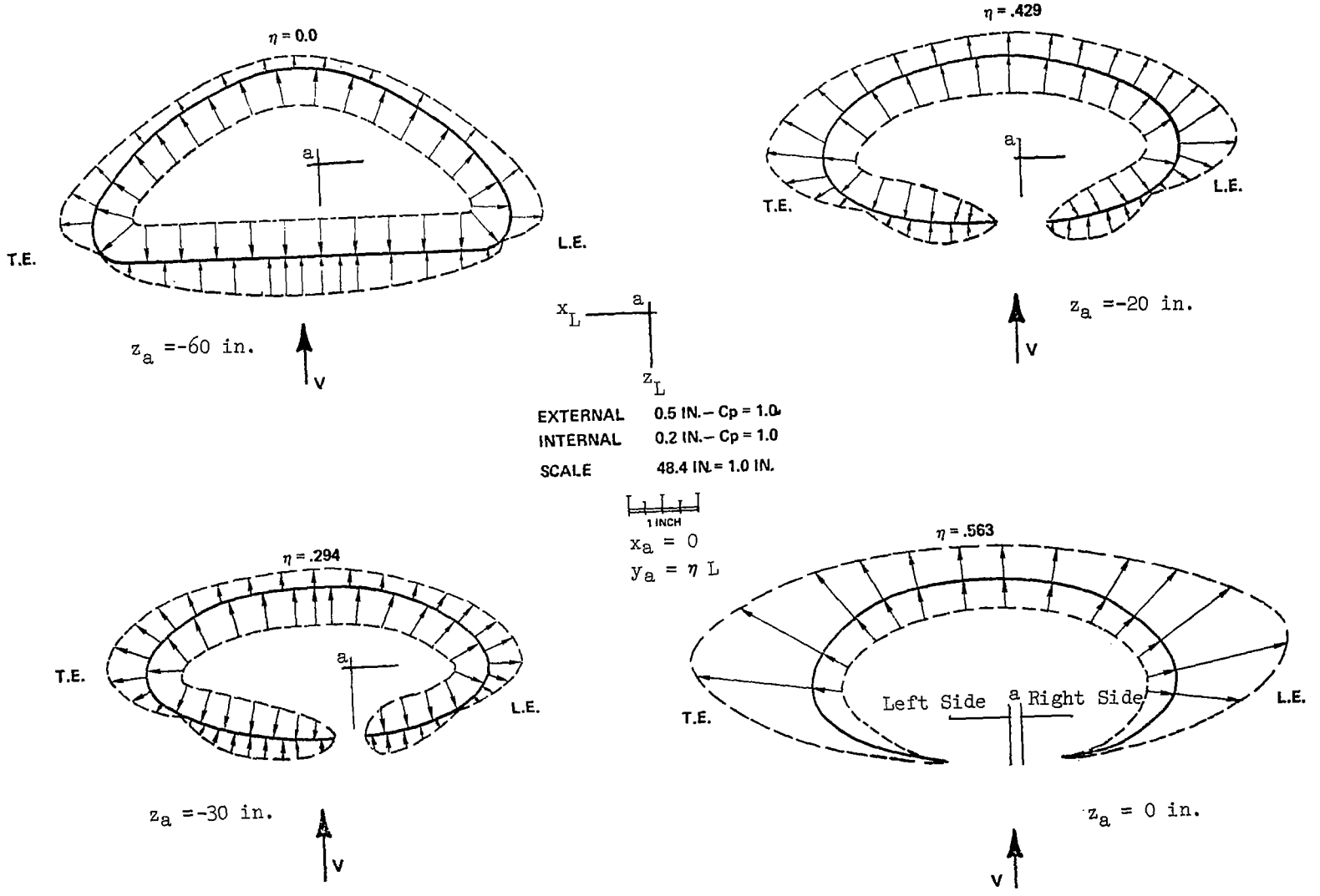

(d) Pressure distributions, left lobe (right lobe similar).

Figure 17.- Continued.

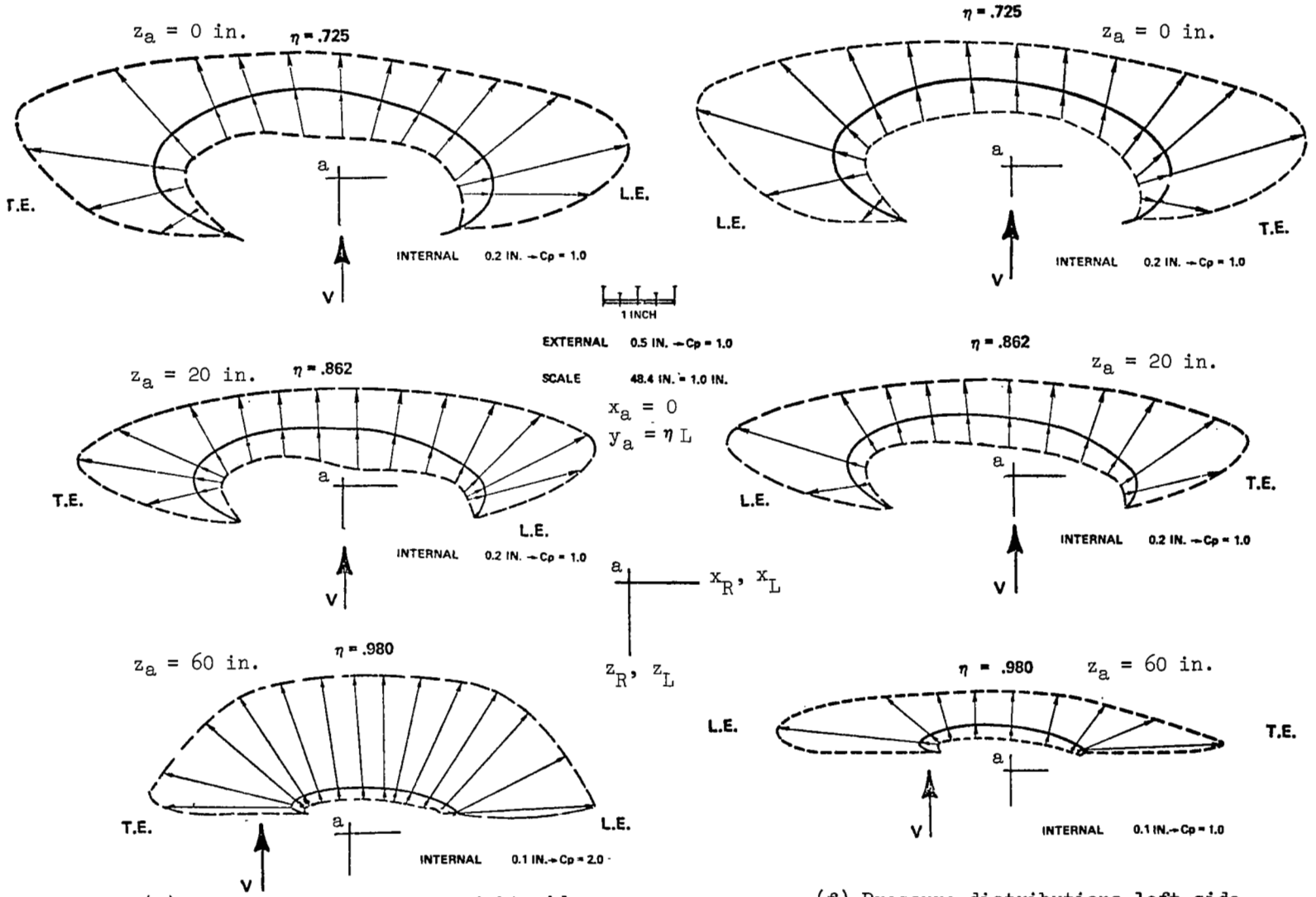

(e) Pressure distributions, right side.

(f) Pressure distributions, left side.

Figure 17.- Concluded.

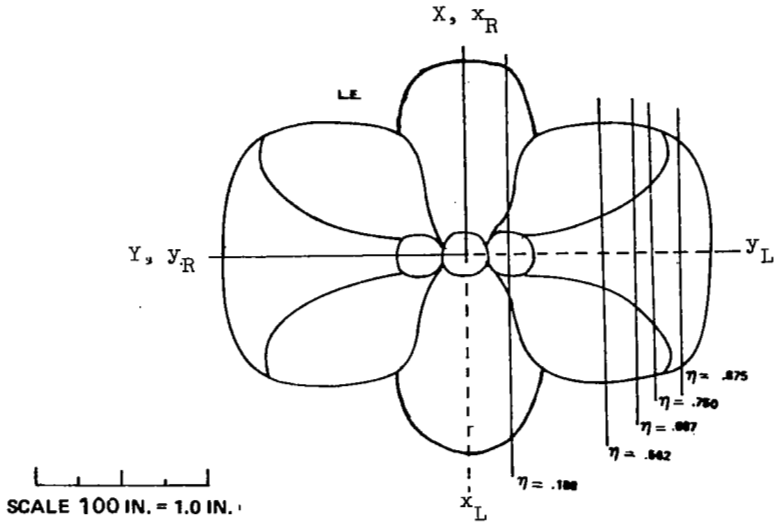

(a) Configuration, bottom view

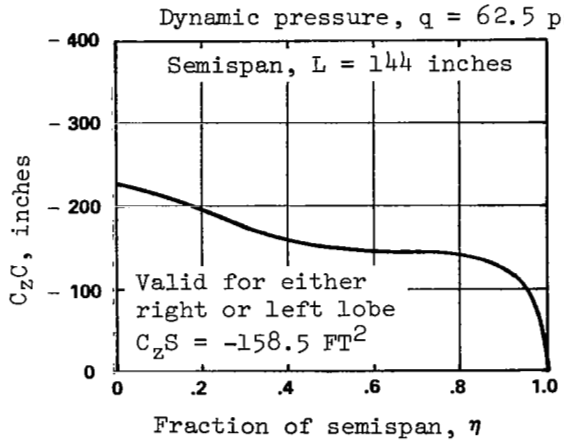

(b) Vertical (z) loading.

Figure 18.- Aerodynamic loading for flight 205-T at first stage inflation, 28.72 seconds elapsed time.

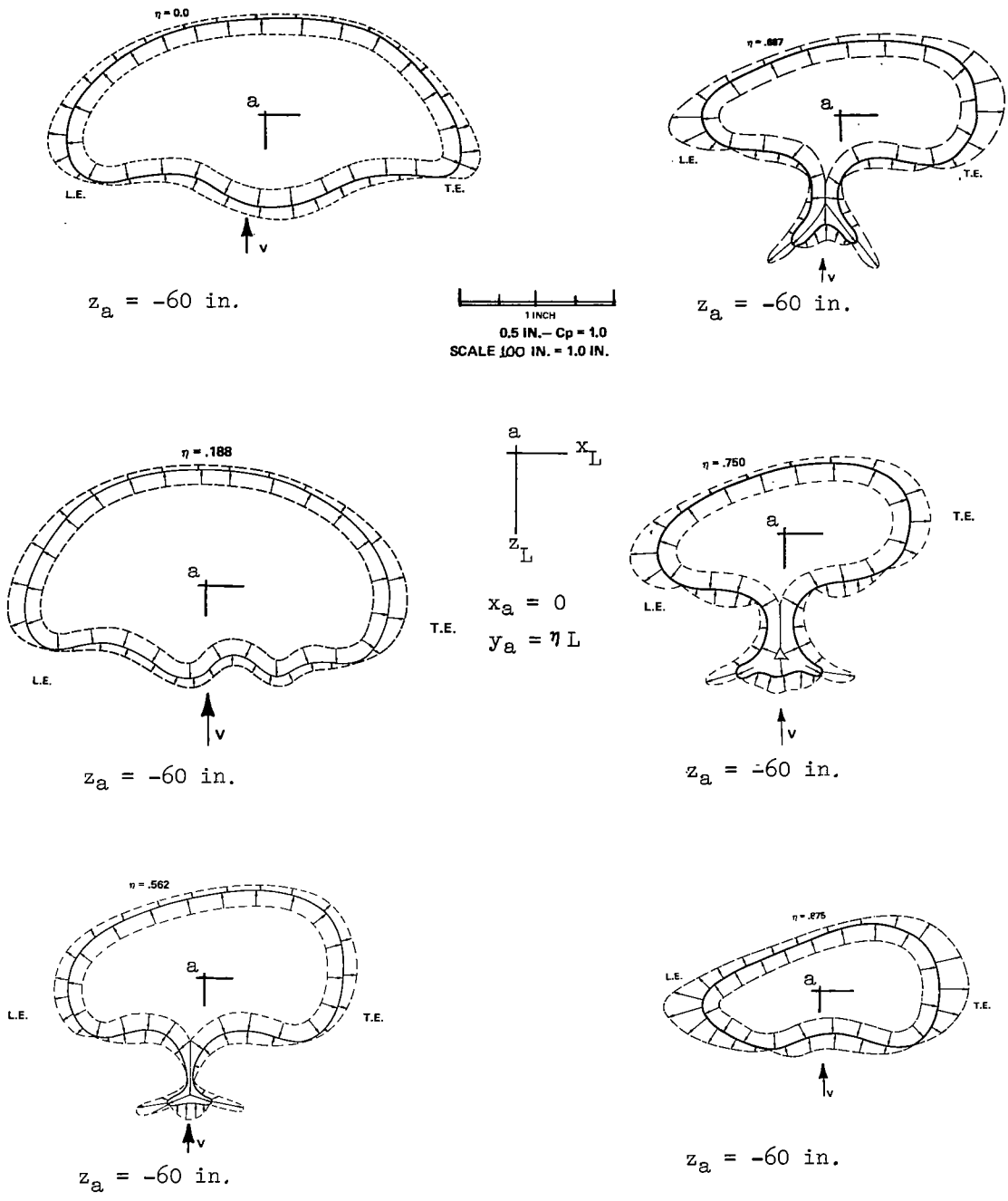

(c) Pressure distributions, left lobe (right lobe similar)

Figure 18. - Concluded.

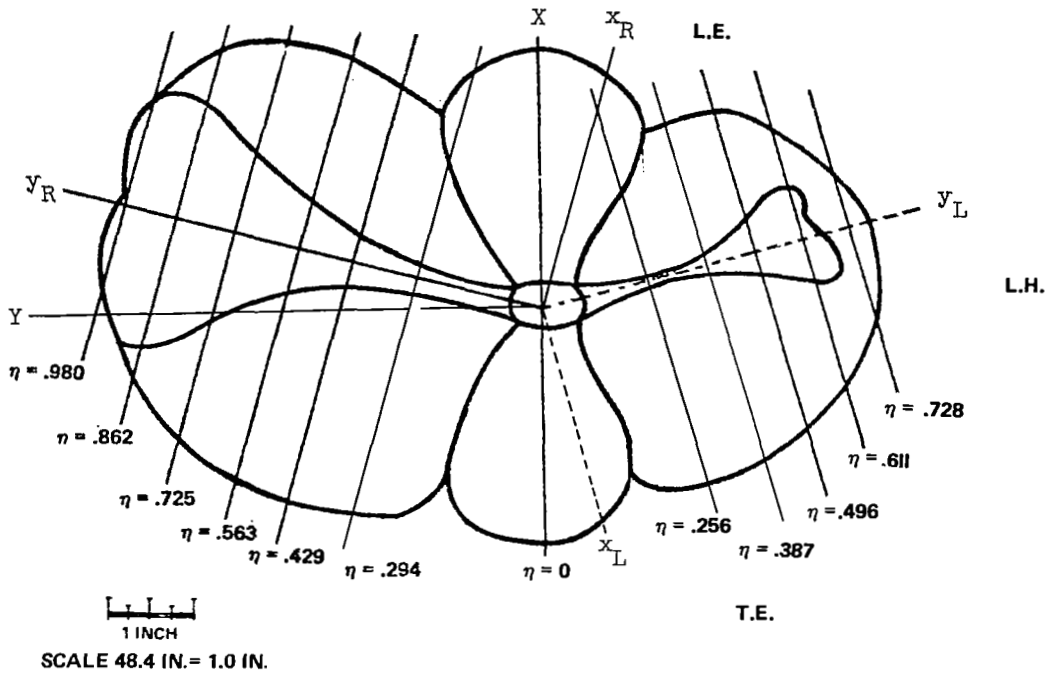

(a) Configuration, bottom view.

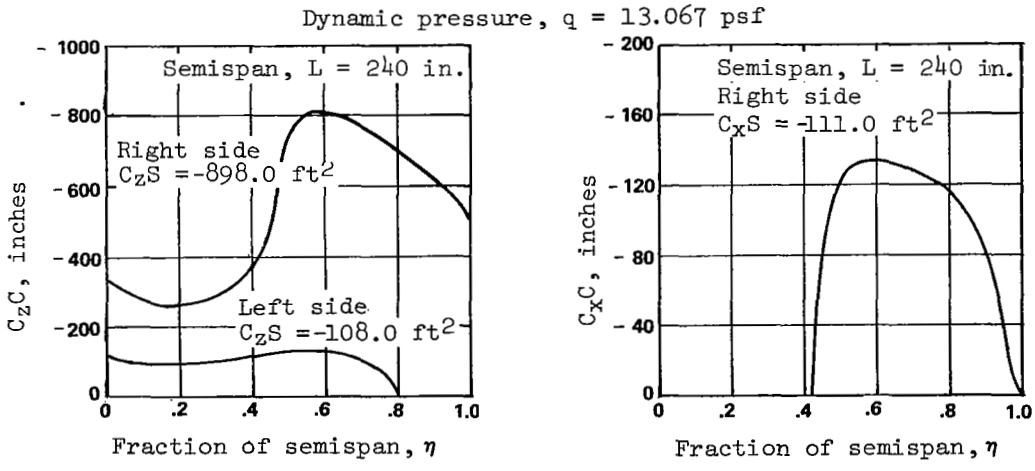

(b) Vertical (z) loading.

(c) Chordwise (x) loading.

Figure 19.- Aerodynamic loading for flight 205-T at second stage inflation, 34.28 seconds elapsed time.

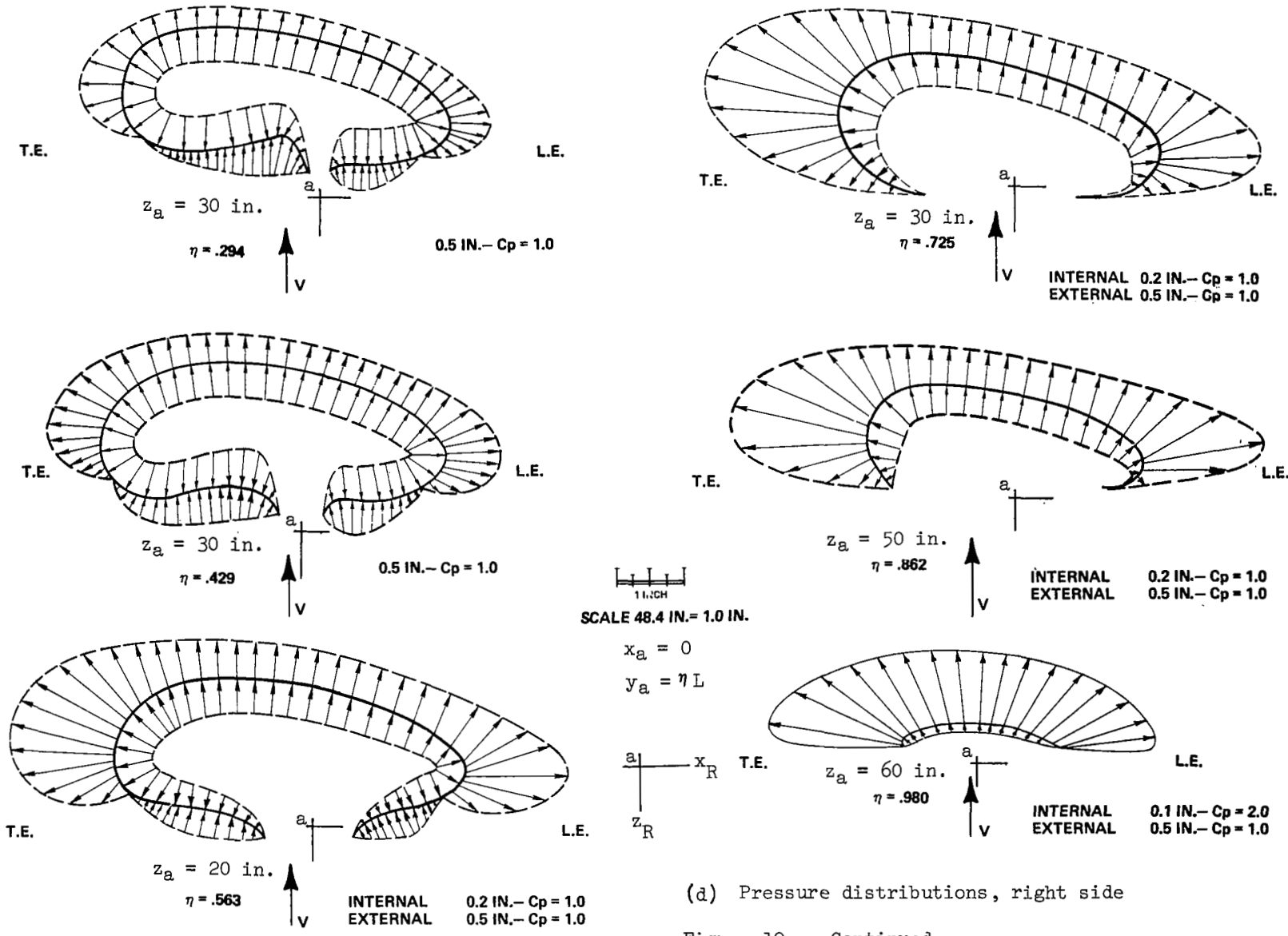

(d) Pressure distributions, right side

Figure 19. - Continued.

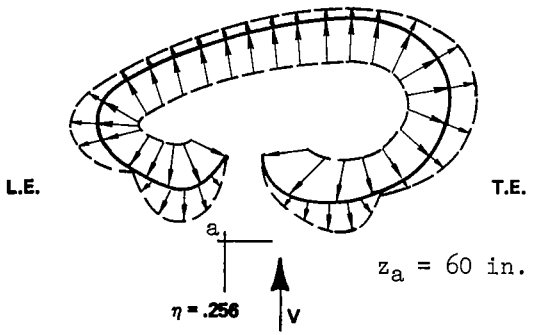

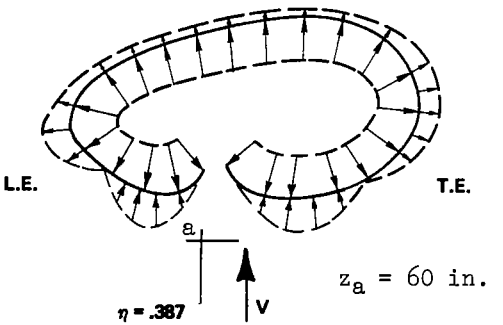

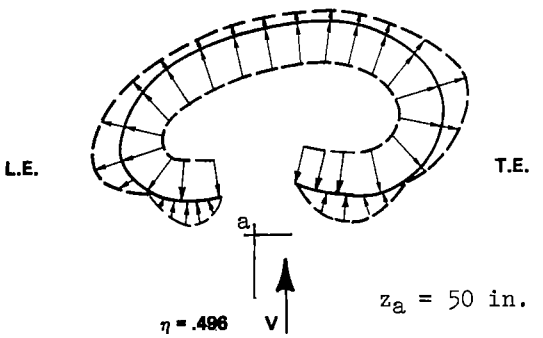

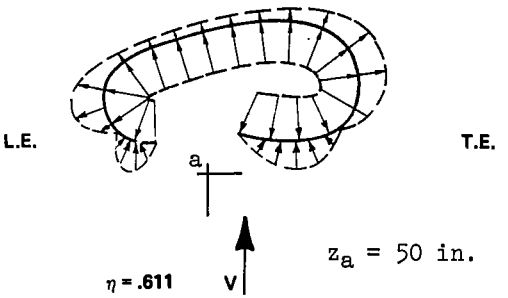

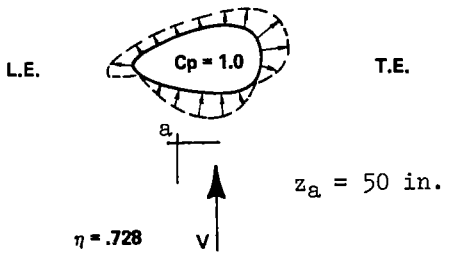

0.5 IN.– Cp = 1.0

SCALE 48.4 IN.= 1.0 IN.

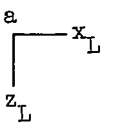

$x_a = 0$

$y_a = \eta L$

(e) Pressure distributions, left side.

Figure 19.- Concluded.

CONCLUSIONS

Geometric, kinematic, and aerodynamic data characterizing the deployment of two NASA parawings (203-T and 205-T) have been established from photographic, telemetry, and Askania data acquired from flight tests of the wings. These data are essential in support of proposed finite element structural analyses of the parawing. The mold-loft lines are needed to construct a finite element model of the structure. The kinematic data are required in the development of the aerodynamic pressure distributions and the body forces due to inertial reactions.

The data processing required prudent estimates and extensive engineering judgement. Approximate procedures were necessitated by the absence of information on the positions of the cameras relative to the range coordinate system, the lack of sufficient identifiable marking on the canopy and suspension lines, the lack of overhead film coverage, and the absence of timing marks on the photographic records.

No measurable data on line motions could be obtained due to the inability to observe the end motions for adequate time intervals and the lack of identifiable intermediate points. Color marking of quarter points might have made identification of these points possible.

The three dimensional characteristics of the parawing geometry could not be rigorously computed because of the absence of positional data on the cameras involved. This, coupled with the lack of sufficient identifiable marking on the canopy, and the lack of overhead coverage necessitated the use of a scale model to aid in the development of the mold loft lines.

The time phasing of the various films was difficult, and in some cases inaccurate, because of the lack of timing marks on the data and the variations in camera speeds from the nominal.

Camera speeds of 100 frames per second were insufficient to provide accurate information on accelerations of specific canopy points during the sudden termination of inflation.

The critical loading conditions for both flights occurred during second stage inflation. Large pressure coefficients were identified as resulting from the arresting of flow by the sudden termination of motions associated with the inflations. These transient aerodynamics produced pressure differentials as high as five times the dynamic pressure of the free stream. The structural failure of flight 203-T is believed to be the result of the impulsive arresting of the spanwise expansion of the right lobe. On the other hand, the structural failure of 205-T appears to be caused by the aerodynamic transients resulting from an abrupt reversal in curvature of the right lobe during its chordwise expansion.

Between the two flights, the maximum accelerations associated with the termination of the second stage deployment had spanwise magnitudes near 200 g's and chordwise magnitudes slightly over 100 g's.

The opening processes associated with second stage inflation are not symmetrical and are thought to be the result of improper behavior of the first stage reefing lines as they are drawn through the reefing rings on the side lobe leading edges. Since both lines have to draw a terminal eyelet through the reefing rings, it seems likely that the eyelet will become temporarily lodged from time to time. In general, this would imply an essentially random behavior during second stage inflation.

The resultant aerodynamic force components computed from the estimated aerodynamic pressure distributions showed good agreement with force components derived from the onboard accelerometers.

More accurate data processing could be achieved by:

(a) Higher speed cameras for few seconds of inflation process.
(b) Use of identifiable colored markings on canopy and lines.
(c) Making flight tests on days when carefully controlled atmospheric conditions are achieved.
(d) Use of fine grain photographic development techniques.
(e) Recording coordinates of camera locations and optical characteristics of the camera.
(f) Including calculations of elevation, azimuth and slant range of each camera with the other Askania data.
(g) Locating at least three cameras for good triangulation on the early phase of the drop test.
(h) Use of more instrumented lines.
(i) Placing onboard camera so that instrumented lines can be observed.

APPENDIX A

MOTION ANALYSIS FROM PHOTOGRAPHIC RECORDS:

PROCEDURE AND ERROR ASSESSMENT

The filmed records of the deployment were studied on a visual motion analyzer which provided projection of the 16 mm film on a ground glass working surface. Controls permitted forward and reverse film motion at variable speeds, as well as still projection. A frame counter provided repeatable frame by frame reference.

Overlays on vellum were made of the motions of interest with sufficient detail to identify the instantaneous configuration. Vellum was used to obtain superposition of successive frames and thus the relative motion of points of interest on the canopy. Identification of line attach points and intermediate points on the canopy skirt was facilitated by the contrasting red reinforcement patches at these points against a light parawing background. Displacements of interest were plotted and numerically or graphically differentiated to obtain the velocities and accelerations of particular points.

An attempt was also made to determine suspension line motions during the critical stages of inflation. However, no useful data was obtained for either flight. This was due primarily to the inadequacy of the test vehicle-to-air film in identifying the end motions, and the lack of any identifiable positions along the length of the lines. Future flights should have key lines with color markings at one quarter intervals or flags attached. This is absolutely necessary, as a minimum, for line motion studies.

The most important sources of error in the canopy motion analysis are thought to be the determination of scale factors, the timing of events (timing marks were not provided on the film), and the fore-shortening of dimensions due to camera view angle. The following sections are devoted to a discussion of these error sources.

Scale Factor Determination

The scale factor for the photographic image of an object at a distance, D, along the camera line of sight (slant range) is defined as

$$SF = \frac{A}{a} = \frac{D}{f}, \quad f << D,$$

where A is the true projected length as seen normal to the line of sight, a is the length measured on the film, and f is the focal length of the camera. If the motion analyser is used the relation becomes

$$SF = \frac{D}{f} * M,$$

where M is the magnification factor of the analyzer. Since f and M are known, the scale factor can be determined provided that the slant range is known. The slant range could be readily calculated if the camera coordinates with respect to the range references were recorded. Unfortunately, this information was not available for flights 203-T and 205-T. The scale factor must therefore be estimated by identifying a known length in the photograph. In general, the lack of true-length dimensions of reasonable size,or in the case of the vehicle-to-air films, the lack of any constant true-length dimensions made it difficult to obtain accurate scale factors.

In the ground-to-air films in which the canopy was viewed directly overhead, the test vehicle bomb diameter and flare diameter were available for true-length measurement. In general, such measurements made from the ground glass screen of the visual analyzer were less precise than those made from the 70-mm still photograph sequences. The error involved in measuring bomb diameter from still sequences is taken to be $\pm$ .020 inch, and from the ground glass screen of the visual analyzer $\pm$ .040 inch. Where bomb diameter is the only true length available,the error of measurement can be considerable; for instance in the worst possible case:

$$\% \text{ error} = \frac{.040 \text{ inch error} * 100}{.250 \text{ inch bomb dia.}} = \pm 16\%$$

In film sequences in which a line appeared approximately normal to the line of sight, much better scale factor accuracy was attained. The use of a true-length view of a parawing suspension line 516 inches in actual length vs a 36 inch bomb diameter provided a reduction of measurement error to 1/15 of that cited above ,about 1.0%. Care should be taken not to determine the scale factor from a line length at high loading unless the length is corrected for stretch. Neglect of stretch may result in an error in scale factor as high as 10%.

In the case of the vehicle-to-air film sequences, there was no dimension of true length from which a reasonably accurate scale factor could be determined. However, the overall dimension of the reefed center lobe was determined from ground to air sequences at second stage inflation. Since this dimension was found to be relatively constant, a ratio of the center lobe dimension scaled from the ground-to-air film and the vehicle-to-air film was used to provide a scale factor for views taken by the camera in the test vehicle.

$$SF_{v/a} = SF_{g/a} \left(C_{g/a}/C_{v/a}\right)$$

where: SF = scale factor
C = Center wing (reefed) fore-aft dimension measured on the film
g/a = ground-to-air
v/a = vehicle-to-air

The corresponding dimension from the still photo sequences was used to check the result. These showed a reasonable agreement, that is, within 5%.

The change in altitude from first disreef line-cut to line transfer was 4.75%. Error due to camera approach was minimized in general by determining the scale factor for each period of interest being analyzed. The effect of horizontal translation away from or toward the camera was in general negligible for the small time periods of interest.

Film Speeds and Timing of Events

The times given in Table 1 for the occurrence of particular events were correlated with visual evidence to determine film speeds. In general, the film speeds analyzed correlated reasonably well with the nominal. An exception was the vehicle-to-air sequences where the nominal camera speed of 200 frames per second was found to be in error.

Vehicle to air camera speed - The number of frames between program chute disconnect and line transfer can be precisely determined from the test vehicle camera records, since the occurrence of these events is recorded by the appearance of smoke when the initiating squib is fired. For 203-T, this number was 2059 frames. It follows that the average camera speed during this time interval was

$$CS = \frac{2059 \text{ frames}}{(45.234 - 27.357) \text{ sec.}} = \frac{2059}{17.877} = 115 \text{ frames/sec.}$$

In flight 205-T, the interval of squib-to-squib first smoke yielded the same camera speed:

$$CS = \frac{2058 \text{ frames}}{44.163 - 26.246 \text{ sec.}} = \frac{2058}{17.817} = 115 \text{ frames/sec.}$$

Camera speeds calculated for subset intervals indicated that the camera speed was steady for the vehicle-to-air films.

Ground to air Sequences - In correlating film events precisely with Askania event data, some difficulty was experienced due to the possible delay between reefing line cut and subsequent first visible motion for the various disreef stages. Consider, for example, the selection of the configuration (i.e., photo frame) corresponding to the peak vehicle decelerations during 205-T second stage inflation. Two peaks occurred, $\ddot{z}' = 2.60$ g's at 34.28 and $\ddot{z}' = 2.70$ g's at 34.64 seconds elapsed time.

Based on a nominal camera speed of 100 frames per second, a delay of 0.14 seconds ensues between line cut and the first visible motion. This places the critical frame at 0.18 seconds afm. The configuration represented by this frame is shown in Figure 20(a).

A calculation of camera speed based on the frames from program chute disconnect to the beginning of line transfer gave the camera speed at:

$$CS = (F_{lt} - F_{pcd}) / (t_{lt} - t_{pcd})$$

where: F = frame
t = time
lt = line transfer
pcd = program chute disconnect

CS = (2570 - 723) frames/17.917 sec. = 103 frames/sec.

Calculating the frame of first disreef line-cut referenced to program chute disconnect at this camera speed gives the line-cut frame number as:

$$F_{lc} = (t_{lc} - t_{pcd}) \ (CS) + F_{pcd}$$

where: lc = line cut
pcd = program chute disconnect

$$F_{lc} = (33.956 - 26.246 \text{ sec. elapsed time}) \ (103 \text{ frames/sec}) + F_{pcd}$$

$$F_{lc} = 7.71 \text{ sec } (103) + 723 = 1514$$

This calculation, which added 21 frames to the 1494 frames at nominal camera speed, places line-cut at 6 frames after first visible motion on the film and is therefore rejected. If, however, first visible motion were taken to be equivalent to line-cut, the configuration which should represent the first peak vehicle deceleration is shown in Figure 20(b). Since there were two peaks, 2.60 and 2.70 g's, during this stage of inflation, it appears that the nominal camera speed calculated gives a reasonable correlation of configuration with vehicle decelerations. Figure 20(c) shows the second peak, $\ddot{z}' = 2.7$ g's at 0.54 second after first motion, when the transverse canopy skirt-point L3 displacement is completed, the forward canopy edges are inflated, and both trailing edges are continuing to unfurl and inflate.

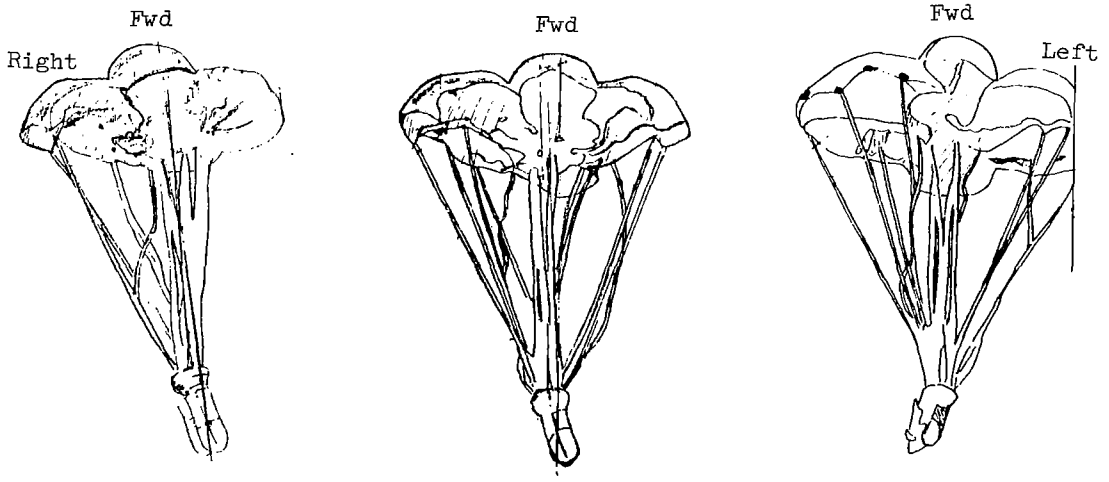

(a) t = 0.18 sec afm (b) t = 0.32 (c) t = 0.54

Figure 20. - Flight 205-T Second Stage Inflation.

Determination of True Dimensions

The kinematic data supplied in the section on "CANOPY MOTION AND AREA" are apparent displacements, velocities, and accelerations since they were not corrected for foreshortening due to viewing angle. Neglect of the foreshortening due to camera orientation results in displacements, velocities, and accelerations being lower than actual values. These data were recorded in this fashion since they are directly reducible from the photographic images and are readily related to the true displacements, velocities, and accelerations by a scalar multiplier. In this section the methods for obtaining the correction factors are shown, and the quantities are recorded for the pertinent frames of interest.

Method for obtaining correction factors - Referring to Figure 21, it is assumed that: (1) points 0, 2, 3, 4, and 5 all lie in a plane which is perpendicular to the position vector, $\vec{r}_{01}$, of point 1 with respect to point 0, (2) the true length, L, of $\vec{r}_{01}$ is known along with the overall scale factor (SF) for the camera and motion analyser.

It follows from assumption (2) that the scaled true length of $\vec{r}_{01}$ is given by:

$$r_{01}(t) = \frac{L}{S\ F},$$

and the angle, θ, between the line of sight and $\vec{r}_{01}$ (view (b)) is

$$\theta = \sin^{-1}\left(\frac{r_{01}(a)}{r_{01}(t)}\right)$$

where $r_{01}(a)$ is the projection of $\vec{r}_{01}$ in view (a).

The transformation from the camera frame coordinate system (x, y, z) to the (x_1, y_1, z_1) system is

$$\begin{Bmatrix} x_1 \\ y_1 \\ z_1 \end{Bmatrix} = \begin{bmatrix} \cos\psi & -\sin\psi & 0 \\ \sin\psi & \cos\psi & 0 \\ 0 & 0 & 1 \end{bmatrix} \begin{Bmatrix} x \\ y \\ z \end{Bmatrix}, \qquad (1)$$

where the angle ψ is measured directly from view (a). The transformation from the $(x_1\ y_1\ z_1)$ system to the system $(x_2\ y_2\ z_2)$, view (c)), in which the true length $r(t)$ of any line in the plane normal to $\vec{r}_{01}$ is defined, is given by

$$\begin{Bmatrix} x_2 \\ y_2 \\ z_2 \end{Bmatrix} = \begin{bmatrix} \cos\theta & 0 & -\sin\theta \\ 0 & 1 & 0 \\ \sin\theta & 0 & \cos\theta \end{bmatrix} \begin{Bmatrix} x_1 \\ y_1 \\ z_1 \end{Bmatrix} \qquad (2)$$

Now $z_2 = 0$ for points 0, 2, 3, 4 and 5 by virtue of assumption 1 (view (b)). Hence, from equation (2) and the third row of equation (1),

$$z_1 = z = -x_1 \tan\theta \qquad (3)$$

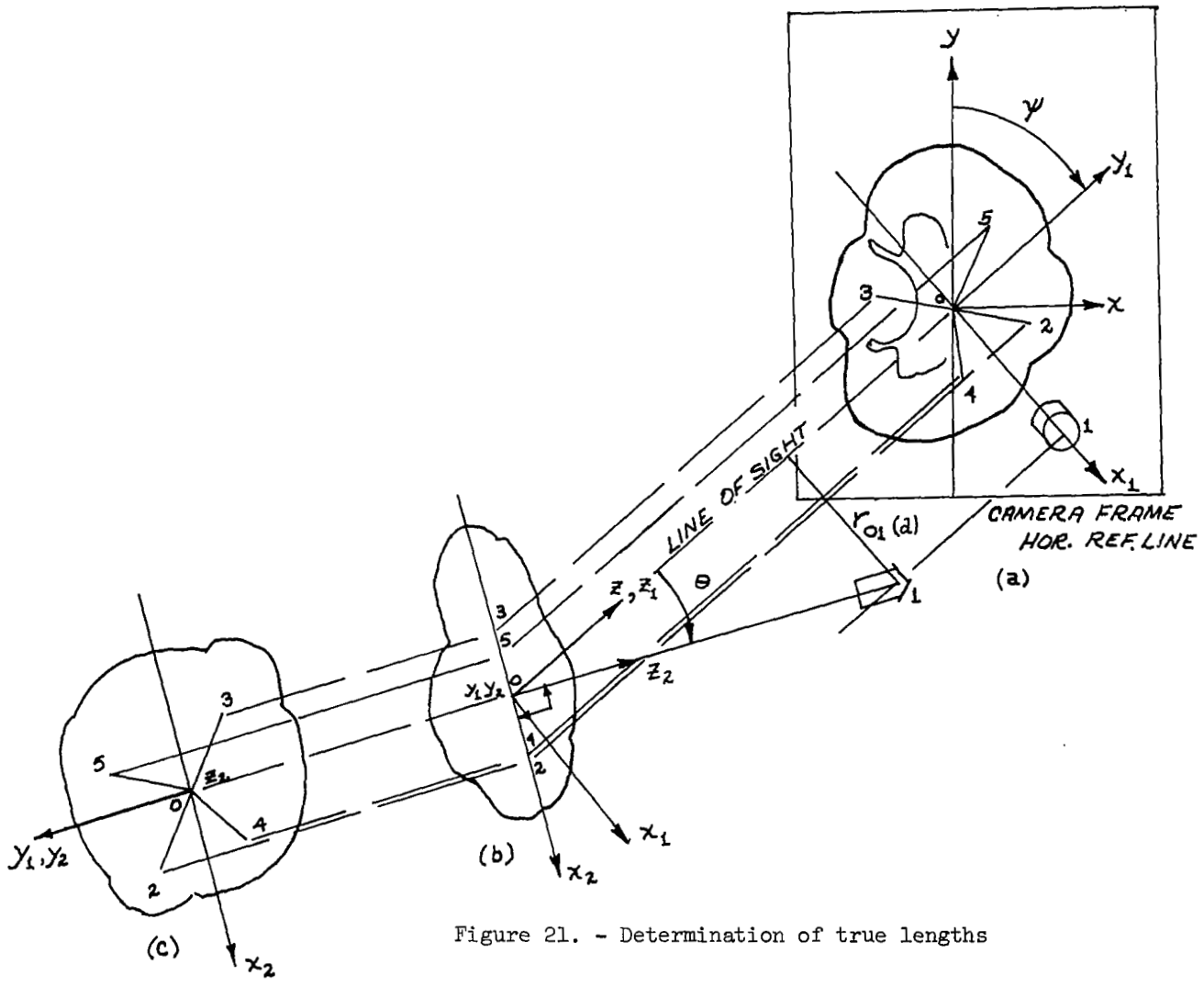

Figure 21. - Determination of true lengths

Substituting equation (3) for z_1 in equation (2) and deleting the third row, since z_2 is always zero, gives

$$\begin{Bmatrix} x_2 \\ y_2 \end{Bmatrix} = \begin{bmatrix} \cos\theta + \sin\theta \tan\theta & 0 \\ 0 & 1 \end{bmatrix} \begin{Bmatrix} x_1 \\ y_1 \end{Bmatrix} \tag{4}$$

Now x_1 and y_1 can be obtained directly from equation (1) because they are not dependent upon the unknown z, thus

$$\begin{Bmatrix} x_2 \\ y_2 \end{Bmatrix} = \begin{bmatrix} \cos\theta + \sin\theta & \tan\theta & 0 \\ 0 & & 1 \end{bmatrix} \begin{bmatrix} \cos\psi & -\sin\psi \\ \sin\psi & \cos\psi \end{bmatrix} \begin{Bmatrix} x \\ y \end{Bmatrix} \tag{5}$$

By performing the matrix product, there results;

$$\begin{Bmatrix} x_2 \\ y_2 \end{Bmatrix} = \begin{bmatrix} (\cos\theta \cos\psi + \sin\theta \tan\theta \cos\psi) & (-\cos\theta \sin\psi - \sin\theta \sin\psi \tan\theta) \\ \sin\psi & \cos\psi \end{bmatrix} \begin{Bmatrix} x \\ y \end{Bmatrix}$$

The true length $(r(t))$ follows as; (6)

$$r(t) = \sqrt{x_2^2 + y_2^2} \tag{7}$$

Equation (6) provides the values of x_2 and y_2 for a given point having coordinates x, y as measured in the camera frame, view (a). Equation (7) provides the true length of the desired dimension. When $r(t)$ is multiplied by the scale factor (SF) the true dimension of the full scale object is obtained. The correction factor for camera view angle is the ratio of the true dimension to the measured dimension. It should be noted that the technique presented above is valid only for the constraint that the points of interest lie in a common plane perpendicular to the vector whose true length is known. Furthermore, the method depends upon knowledge of the scale factor. Since the slant range is not known, the scale factor must be estimated by identifying a known length on the photograph. This is inaccurate because of elastic elongations and because of the difficulty of locating a known dimension in its true view.

Results - Camera view angle correction factors were determined for each of the displacement histories of Figures 9 and 10 and are shown on the appropriate figure. These factors are also summarized in Table 10. A comparison of the maximum corrected displacements is also presented, together with averages for the two flights and % deviation from the average. The latter are presented as a measure of the possible error in displacement resulting from the analysis. It should be noted, however, that the critical velocities, which are a major objective of the analysis, are relatively uneffected by the overall errors in maximum displacement, since the velocities are obtained by differences in local displacements during small time intervals.

TABLE 10 MAXIMUM DISPLACEMENTS

Flight	Item	Measured Displacement (feet)	View Correction Factor	Maximum Corrected Displacement (feet)	Deviation From Average
Second Stage Inflation:					
203-T	r_y (R3)	16.6	1.032	17.2	
205-T	r_y (R3)	16.2	1.060	17.2	
Average				17.2	0.0%
203-T	r_y (L3)	17.0	1.040	17.8	
205-T	r_y (L3)	13.4	1.013	13.6	
Average				15.7	12.1%
203-T	r_x	9.0	1.030	9.26	
205-T	r_x	10.0	1.043	10.43	
Average				9.84	5.9%
Third Stage Inflation:					
203-T	r_x	16.6	1.124	18.7	
205-T	r_x	21.5	1.145	24.6	
Average				21.65	13.6%
Fourth Stage Inflation:					
203-T	r_y	36 ft.	1.0	36 ft.	

The average values of the maximum spanwise displacement agreed fairly well with the theoretical diameter of inflated right and left hand lobes (16.8 feet) at the completion of second stage inflation. Although good agreement was obtained for spanwise displacement of R3 and L3 for flight 203-T (17.2 feet vs 17.8 feet), a disparity resulted for the 205-T flight, (17.8 vs 13.6 feet). This disparity existed in the raw data and is due to the ambiguity of the location of the centroid of the center lobe inlet used as a reference from which to measure the transverse displacements.

The 13.6% deviation of canopy displacements from the average during third inflation is probably due to the ripped panel in flight 203-T.

REFERENCES

1. Rogallo, Francis M., Lowry, John G., Croom, Delwin R., and Taylor, Robert T.: Preliminary Investigation of a Paraglider. NASA TND-443, 1960.

2. Sleeman, W. C., Jr., and Gainer, Thomas G.: Status of Research on Parawing Lifting Decelerators. Preprint 68-967, Am. Inst. Aeron. and Astronaut., September 1968.

3. Gainer, Thomas G.: Investigation of Opening Characteristics of an All-Flexible Parawing. NASA TND-5031, 1969.

4. Moore, Robert H., Eichblatt, David L., and Hughes, Theodore F., Experimental Scale Factors for Parawing Opening Characteristics with Dimensional Ratios from 1:1.3 to 1:3. NASA TND-5071, 1969.

5. Polhamus, Edward C., Geller, Edward W., and Grunwald, Kalman J., Pressure and Force Characteristics of Non-Circular Cylinders as Affected by Reynolds Number with a Method Included for Determining the Potential Flow About Arbitrary Shapes. NASA TR-R-46, 1959.

6. Melzig, H. D., and Schmidt, P. K., Pressure Distribution During Parachute Opening, Phase I - Infinite Mass Operating Case. AFFDL-TR-66-10, 1966.

7. Shapiro, Ascher H., The Dynamics and Thermodynamics of Compressible Fluid Flow. Vol. I, The Ronald Press Co., 1953.

NASA-Langley, 1971 —— 32 CR-1788